R-12-11

Iron hydroxide occurrences and redox capacity in bedrock fractures in the vicinity of SFR

Björn Sandström, WSP Sverige AB

Eva-Lena Tullborg, Terralogica AB

Magnus Sidborn, Kemakta Konsult AB

December 2014

Svensk Kärnbränslehantering AB
Swedish Nuclear Fuel
and Waste Management Co

Box 250, SE-101 24 Stockholm
Phone +46 8 459 84 00

ISSN 1402-3091
SKB R-12-11
ID 1364488

Iron hydroxide occurrences and redox capacity in bedrock fractures in the vicinity of SFR

Björn Sandström, WSP Sverige AB

Eva-Lena Tullborg, Terralogica AB

Magnus Sidborn, Kemakta Konsult AB

December 2014

Keywords: SFR, Forsmark, Redox, Mössbauer, Geology, Fracture mineralogy, Redox capacity.

This report concerns a study which was conducted for SKB. The conclusions and viewpoints presented in the report are those of the authors. SKB may draw modified conclusions, based on additional literature sources and/or expert opinions.

A pdf version of this document can be downloaded from www.skb.se.

Summary

The observation of many apparent occurrences of Fe(III) hydroxide in the mineral data of the fracture data set used in the hydrogeochemical SDM of SFR prompted some additional work. There were both analytical doubts about the extent and existence of this iron minerals and concerns for their implication as potential redox indicators and markers of relatively late oxygenated water infiltration at greater depths. This is of particular importance, as the redox state of the repository is evaluated in the present safety analysis for the SFR extension project (SR-PSU). The fracture mineral data in Sicada are collected during the drill core mapping and it is often difficult to visually distinguish between iron hydroxide and iron rich clay minerals and hematite-stained minerals. Therefore, a detailed investigation of fractures mapped as iron hydroxide-bearing in Sicada was initiated. In order to reduce the number of boreholes investigated for this study and to obtain data representative from all levels of the bedrock, the following borehole were selected for investigation: KFR102B, KFR103, KFR104 and KFR106

A total number of 61 fractures mapped (after macroscopic inspection) as iron hydroxide in boreholes KFR102B, KFR103, KFR104 and KFR106 in Sicada, were revisited. The occurrences in these boreholes represent all depths down to –325 m.a.s.l.. After detailed fracture mineralogical identification, only two of these fractures were inferred to potentially contain iron hydroxide. The minerals most often mistaken for iron hydroxide in these drill cores are iron-rich mixed layer clay, uranium-minerals and hematite-stained adularia and albite. A few fractures mapped as iron hydroxide-bearing contained rust-coloured metallic iron from the drilling process.

In addition, this report presents quantitative data of the available redox capacity in form of Fe(II) in fracture filling material based on statistical analysis Mössbauer and geochemical analyses.

Sammanfattning

En kompletterande studie inleddes på grund av att datamängden av sprickmineral inom SFR hydrogeokemisk platsbeskrivning (SDM), innehöll många förekomster av järnhydroxid också till större djup än inom platsundersökningen för Forsmark. Det är svårt att säkert identifiera järnhydroxid makroskopiskt och för att vara säker behövs oftast en mer detaljerad analys än vad som ingår i den reguljära karteringen. Järnhydroxid kan tyda på oxiderande förhållanden under sen tid och kan därför vara en indikation på infiltration av syresatta vatten. Kunskapen om redoxförhållanden på förvarsdjup är därför en viktig faktor för kommande säkerhetsanalyser samt nu pågående för projektet SFR utbyggnad (SR-PSU). Sprickmineralogidata i Sicada samlas in under borrkärnekarteringen och det är svårt att okulärt skilja mellan järnhydroxid och järnrika lermineral och mineral färgade av hematit. Därför initierades en undersökning av sprickor som karterats som järnhydroxidförande. För att reducera antalet undersökta sprickor och erhålla data som representerade samtliga nivåer, valdes följande borrhål ut för undersökningarna: KFR102B, KFR103, KFR104 och KFR106.

Totalt hade 61 sprickor (efter okulär besiktning) karterats som järnhydroxidförande i borrhål KFR102B, KFR103, KFR104 and KFR106 och inlagrats i Sicada. Förekomsterna representerar alla djup ner till –325 m.ö.h. Efter detaljerade undersökningar kvarstod bara fem som potentiellt järnhydroxidförande. De vanligaste mineralen som misstagits för järnhydroxid i dessa borrkärnor är järnrika lermineral, uranmineral samt adularia och albit färgad av hematit. Ett fåtal sprickor karterade som järnhydroxid-förande innehöll rostfärgade metallfragment från borrprocessen och representerade alltså artefakter

Dessutom presenteras i denna rapport kvantitativ data av den tillgängliga redoxkapaciteten i sprickfyllnader i form av Fe(II), baserat på statistisk analys av Mössbauer och geokemisk data.

Contents

1 Introduction

This report is part of the complementary site investigations for the future expansion of SFR. The report presents an investigation of the occurrence of iron hydroxide in bedrock fractures and a statistical analysis of the quantitative redox capacity provided by the fracture minerals present within the SFR fracture system. The end user of the data is the SFR safety assessment. The data have been obtained from drill core samples. The locations of the boreholes are presented in Figure 1-1.

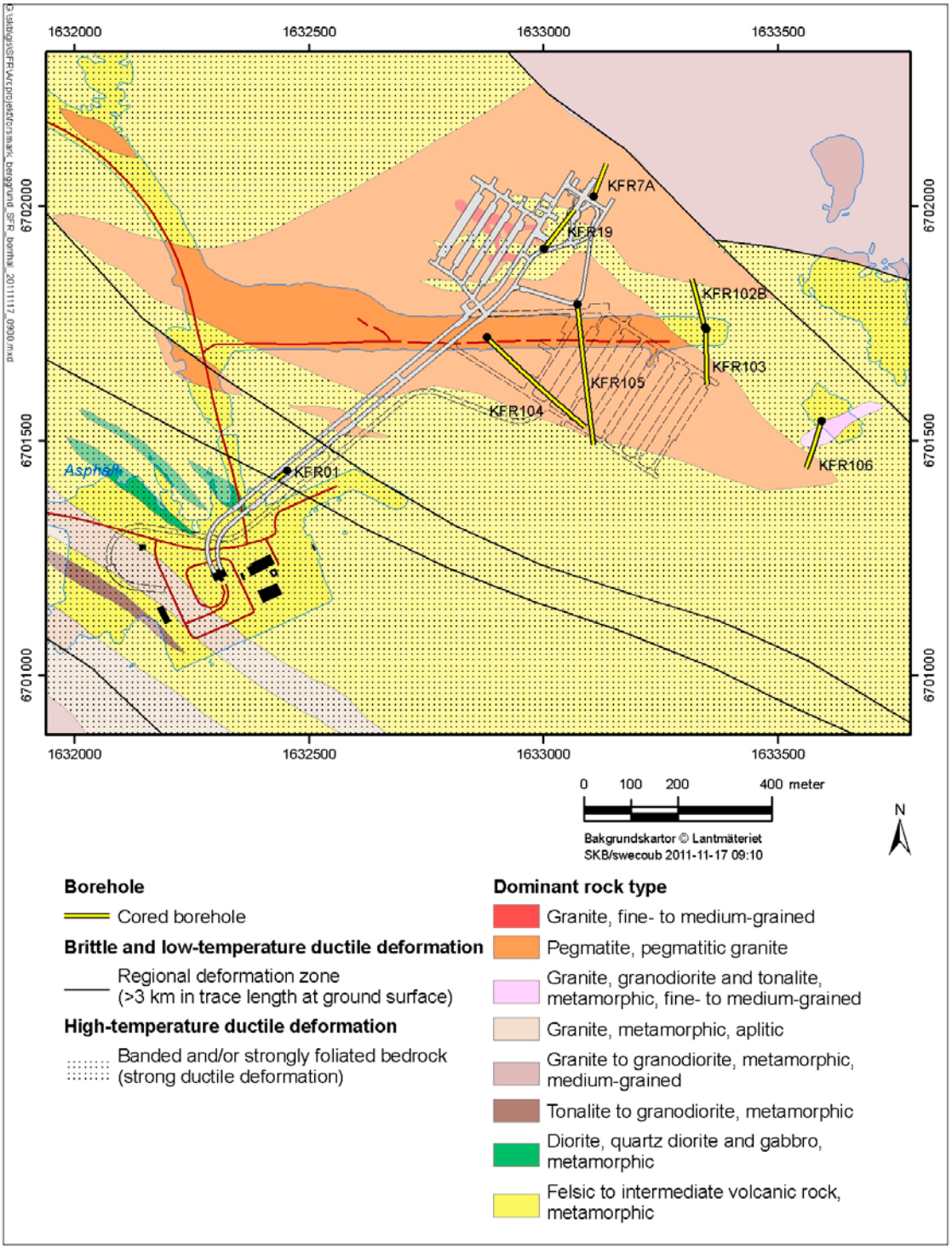

Figure 1-1. *Bedrock geology of the SFR area with surface projection of the sampled boreholes.*

The controlling documents for performing the activity are listed in Table 1-1. Both Activity plan number and Method description are SKB's internal documents. Original data from the reported activities are stored in the primary database Sicada where data are traceable by the Activity Plan number (AP SFR-11-002). Only data in these databases are accepted for further interpretation and modelling and therefore the data presented in this report represent copies of the original data. Data in the databases may be revised, if needed, albeit this will not necessarily result in a revision of the P-report, although this is the normal procedure in case of major revisions. Minor revisions are normally presented as supplements available at www.skb.se.

Table 1-1. Controlling documents for the performance of the activity.

Activity plan	**Number**	**Version**
Bestämning av redoxkapaciteten i sprickmineral och förekomster av järnhydroxider i SFR	AP SFR-11-002	1.0
Method description	**Number**	**Version**
Metodbeskrivning för sprickmineralanalys	SKB MD 144.000	1.0

2 Background

2.1 Observations of redox conditions in bedrock

The following summary of redox conditions in the upper part of the bedrock is based on the more thorough review presented in Sidborn et al. (2010) and references therein.

The normally oxidising condition prevailing in surface waters will change due to organic and inorganic processes and become reducing when intruding into the bedrock fracture network and rock matrix. This transition may take place at quite different depths depending on the content of oxidants in the recharge water but also on flow velocity, thickness of soil cover and bedrock properties. Two kinds of boundaries between mainly oxidising to reducing conditions are often present within the bedrock and they can be described as:

1. A *redox front*, defined as a spatially steep gradient of redox conditions within the rock matrix. This type of redox front is generally sharp and can often be seen as a change in colour of the rock due to redox reactions.
1. A *redox transition zone*, defined as where oxidising conditions in the fracture system close to the surface gradually changes into reducing conditions at depth. In the oxidised zone above the transition zone, all parts of the fracture system are under oxidising conditions whereas in the redox transition zone, oxidising and reducing conditions may occur contemporaneously at the same depth but in different channels within the fracture system. Below the lower limit of the transition zone, all parts of the fracture system are under reducing conditions. The position of the transition zone may vary in time, e.g. seasonally.

Direct Eh measurements are very complex and associated with several technical and conceptual problems. Also, mixing of different waters is difficult to avoid in near surface environments. Therefore, secondary evidence such as the spatial distribution of redox sensitive elements (e.g. Fe, Mn, U, S, Ce), fracture minerals (e.g. sulphides, Fe-oxides, Fe-oxyhydroxides) and Uranium-Series Disequilibrium analyses (USD) can be used to detect the depth to which oxidising waters penetrate.

An observed redox transition zone or redox front can be representative for the present situation, i.e. it is reflected in the groundwater/porewater geochemistry and redox reactions are ongoing, or it can be fossil and represent where redox reactions occurred at some period in the hydrogeochemical evolution of the area. The location of a fossil redox transition zone indicates how far oxidising fluids have penetrated the bedrock fracture system at *some time* during the hydrogeological evolution; the same is valid for the location of a fossil redox front in the rock matrix. At a fossil redox transition zone/redox front, a redox gradient is not discernible in the groundwater/porewater. Hence, a fossil redox transition zone/redox front can only be observed by studies of solid phases. Oxidising conditions do not imply that the minerals have been completely oxidised; the degree of mineral oxidation depends on factors such as time, mineral properties and the potential of the oxidising fluid.

2.2 Observations of redox conditions in SFR

During the compilation of fracture mineral data from the Sicada database in connection with the work with the SFR hydrogeochemical site description (SDM), it was noticed that many occurrences of iron hydroxide were present at great depths within the SFR area (Sandström and Tullborg 2011, Nilsson et al. 2011). Iron hydroxides had been mapped in open fractures down to an elevation of –650 m.a.s.l. (Figure 2-1) (Sandström and Tullborg 2011). If only best choice PFL-anomalies were considered, occurrences of iron hydroxide had been mapped down to –190 m.a.s.l. (Figure 2-2) (Nilsson et al. 2011). Observe that data from KFM11A are not included in Figure 2-1. The term iron hydroxide is the mineral name used in Sicada and is therefore used throughout this report for iron oxyhydroxide/goethite.

A detailed description of the geology of the SFR site is presented in Curtis et al. (2011).

Iron hydroxide indicates oxidising conditions and the presence at depth may indicate recent intrusion of oxygenated waters. For the SFR safety assessment, knowledge of the redox conditions at repository depth is an important factor. The fracture mineral data in Sicada are collected during the drill core mapping and it is often difficult to visually distinguish between iron hydroxide and iron rich clay minerals and hematite-stained minerals. Due to the significance of iron hydroxide occurrences at depth for the safety assessment, an investigation of the occurrences of iron hydroxide-bearing fractures at SFR was initiated. A similar investigation was carried out during the Oskarshamn site investigations using the same methodology (Drake and Tullborg 2009).

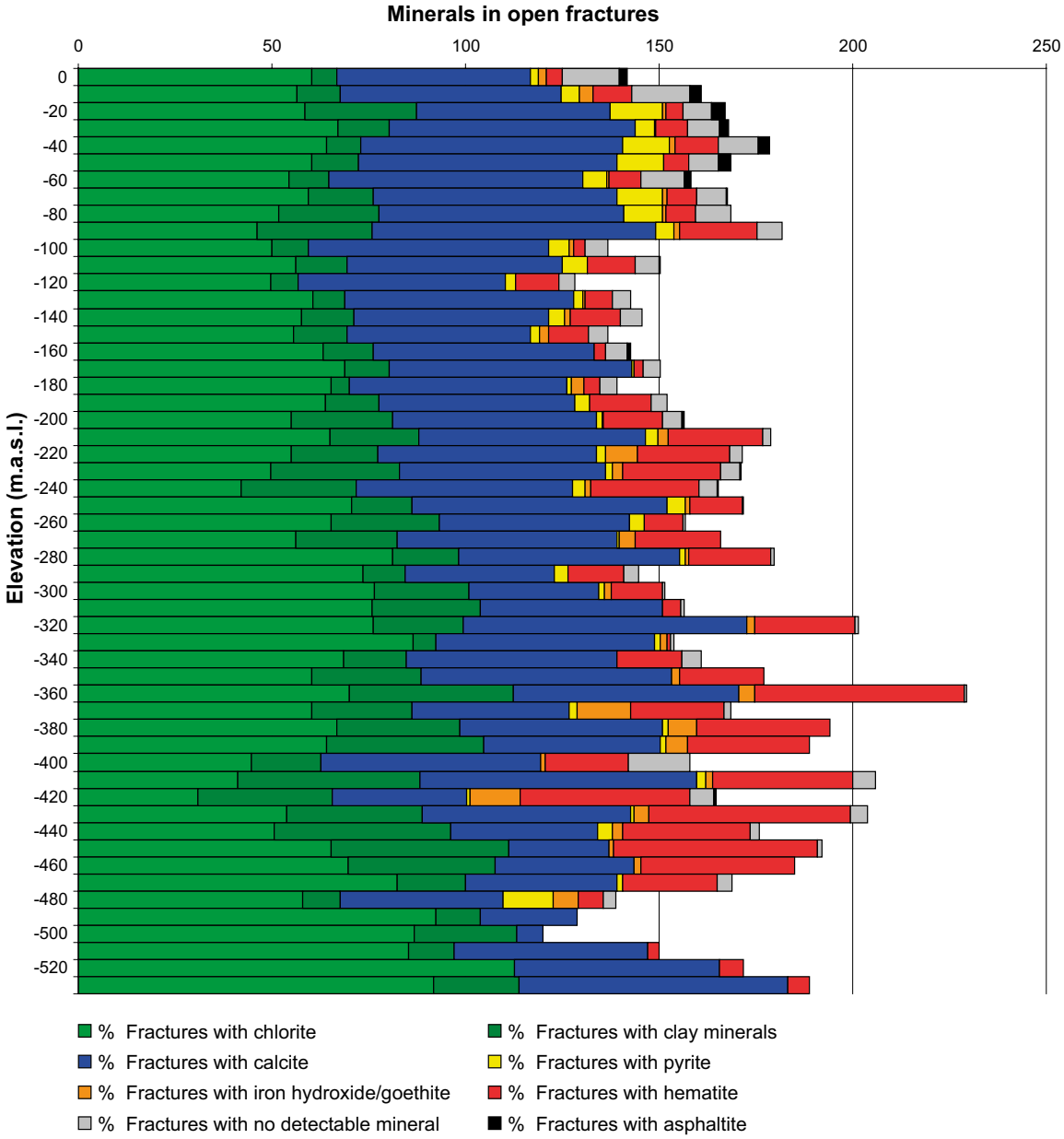

Figure 2-1. *Depth distribution of fracture minerals in all mapped open fractures at SFR. Fractures omitted from the SFR data set are fractures from KFR24 down to Secup 147.50 m where no core was available and fractures from the re-mapped drill cores where no BIPS-logging have been carried out (KFR04, KFR08, KFR09, KFR13, KFR35, KFR36, KFR54, KFR55, KFR7A, KFR7B, KFR7C. Figure adopted from Sandström and Tullborg (2011).*

Hematite occurs frequently in fractures in the SFR drill cores (Figure 2-1 and Figure 2-2) and is indicative for oxidising conditions at the time of its formation. However, the paragenesis associated with hematite is of hydrothermal origin and associated with the Forsmark fracture mineral generations 1 and 2 which are > 1,000 Ma (Sandström et al. 2008, 2009).

The redox state of the repository system is of critical importance for the performance of the SFR extension repository. One of the main disturbances that may occur is the potential ingress of oxidising waters. Therefore, it is relevant to understand if we have indications of previous oxidising events in the bedrock and how the system may buffer these events. In this sense, the quantitative assessment of the redox capacity of the fracture system may be quite relevant.

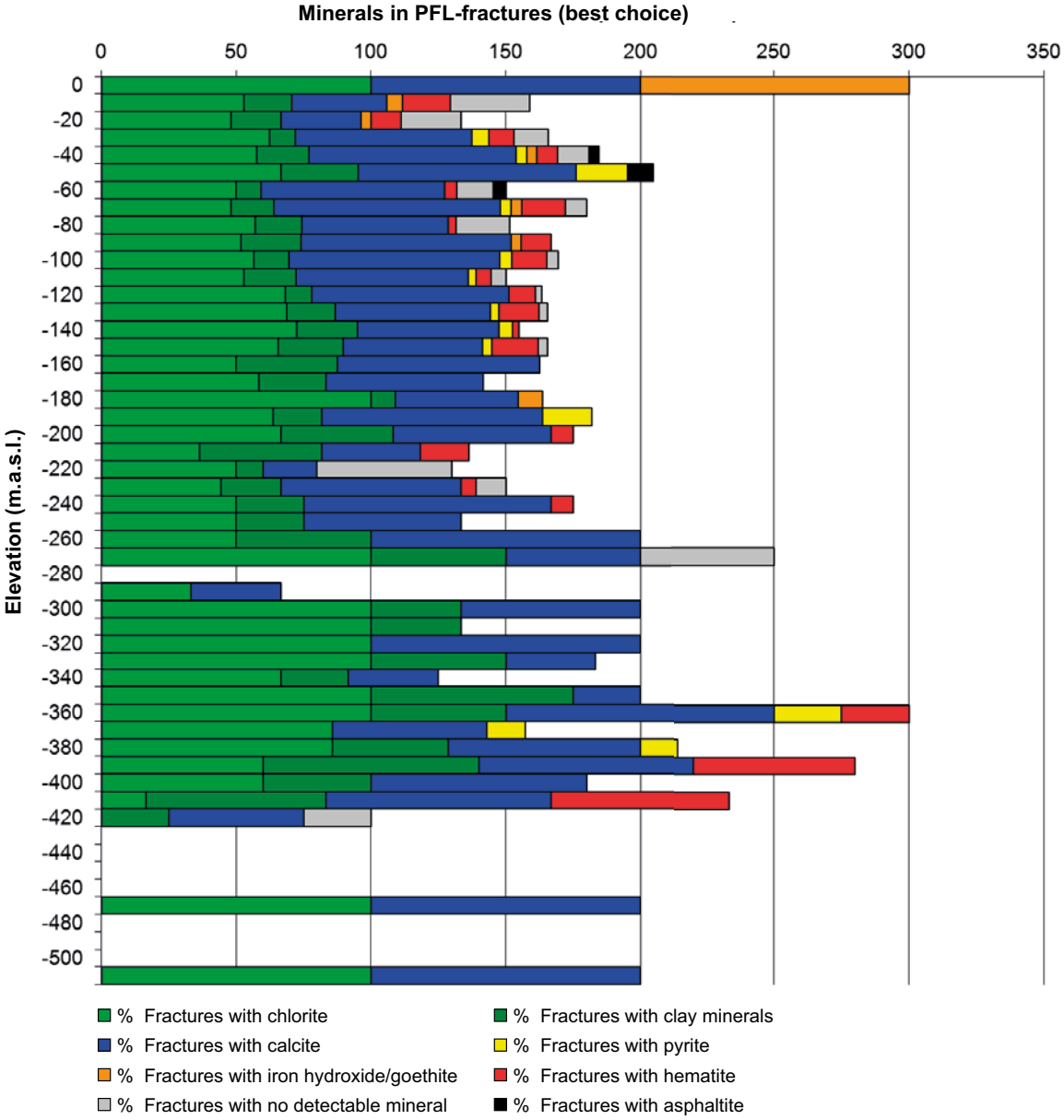

Figure 2-2. *Depth distribution of the fracture mineralogy in all mapped fractures classified as a PFL-anomaly (best choice) from SFR. Only one best choice PFL-fracture has been identified in the uppermost 10 m. The data represent data from the SFR drill cores and KFM11A. Fractures omitted from the SFR data set are fractures from KFR24 down to Secup 147.50 m where no core was available and fractures from the re-mapped drill cores where no BIPS-logging have been carried out (KFR04, KFR08, KFR09, KFR13, KFR35, KFR36, KFR54, KFR55, KFR7A, KFR7B, KFR7C). Between 0 and –5 m.a.s.l., the data are from one single fracture. Figure adopted from Nilsson et al. (2011).*

3 Objective and scope

The objective of this report is to investigate the occurrences of iron hydroxides in fractures and to statistically analyse the quantitative redox capacity present within the SFR fracture system.

The performed analyses during the work with this report are presented in Table 3-1.

Table 3-1. Selected samples and performed geochemical analyses during the work with this report.

Borehole	Secup	Seclow	Fracture Adjusted secup*	Elevation Adjusted secup	SEM–EDS	Mössbauer	ICP–AES/MS
KFR01*	45.18	45.42	n.a.	–87.11		X	
KFR7A*	70.05	70.12	n.a.	–134.73		X	
KFR19*	90.56	90.74	n.a.	–59.22		X	
KFR102B	17.45	17.49	17.452	–11.73	X		
KFR102B	26.76	26.91	26.826	–19.34	X		
KFR102B	113.56	113.88	113.720	–89.61	X	X	X
KFR104	13.22	13.33	n.a.			X	X
KFR104	21.44	21.52	21.504	–14.77	X		
KFR104	21.57	21.66	21.628	–14.88	X		
KFR104	24.80	24.88	n.a.		X		
KFR104	25.03	25.09	25.062	–17.68	X		
KFR104	25.51	25.62	25.568	–18.10	X	X	X
KFR104	27.04	27.11	27.085	–19.34	X		
KFR104	29.80	29.93	29.894	–21.63	X		
KFR104	30.20	30.28	30.241	–21.63	X		
KFR104	32.67	32.76	32.677	–21.91	X		
KFR104	43.53	43.76	43.614	–32.82	X	X	X
KFR104	55.95	56.04	55.968	–42.87	X		
KFR104	59.21	59.25	59.280		X		
KFR104	59.71	59.75	59.729	–45.92	X		
KFR104	61.55	61.93	n.a.		X	X	X
KFR104	99.32	99.42	99.402	–78.03	X		
KFR104	107.64	107.83	n.a.		X	X	X
KFR104	122.52	122.56	122.531	–96.57	X		
KFR104	134.70	134.75	134.719	–106.30	X		
KFR104	270.17	270.23	270.168	–212.46	X		
KFR104	276.60	276.65	n.a.			X	X
KFR104	280.54	280.61	n.a.		X		
KFR104	293.23	293.29	293.461	–230.38	X		
KFR104	294.02	294.15	294.067	–230.84	X		
KFR104	328.75	328.86	328.796	–257.41	X		
KFR104	389.97	390.03	390.013	–303.65	X		
KFR104	416.96	417.35	416.790	–323.66	X	X	X
KFR105*	126.90	127.08	n.a.	–128.37		X	
KFR105*	283.38	283.57	n.a.	–153.22		X	
KFR106	9.72	9.77	9.750	–8.12	X		

*Drill core already sampled for mineralogical and geochemical analysis (Sandström and Tullborg 2011).

4 Execution

4.1 Sample selection

Only cored boreholes from the current SFR drilling campaign drilled with the triple tube technique were selected for sampling due to their higher quality compared to the boreholes drilled during the early investigation and construction of the SFR facility at the nineteen-eighties. In order to reduce the number of boreholes investigated for this study and to obtain data representative from all levels of the bedrock, the following borehole drilled from the surface were selected for further investigation: KFR102B, KFR103, KFR104 and KFR106 (Petersson J 2011, personal communication). Technical data concerning the boreholes are presented in Curtis et al. (2011).

All fractures mapped as iron hydroxide-bearing in Sicada in drill cores KFR102B, KFR103, KFR104 and KFR106 (data delivery Sicada_10_083 (0:1), 2010-06-28) were visually inspected at the core storage (the Lentab hall) at Forsmark. No iron hydroxide-bearing fractures were present in KFR103 Sicada and no sampling of the borehole was carried out. Fractures where the presence of iron-hydroxide could not be excluded based on visual inspection were selected for further analyses. In a few cases when fractures with inferred identical coating mapped as iron hydroxide were present close to each other, only one of the fractures was sampled and set to represent the adjacent fracture(s).

Fractures with enough fracture filling material for Mössbauer analyses (> 40–100 mg) were sampled for quantification of the redox capacity. These were chosen to represent various depths from –18 to –324 m.a.s.l..

Five drill core samples from KFR01, KFR7A, KFR19 and KFR105, which already had been analysed for mineralogy and geochemistry (Sandström and Tullborg 2011) were also selected for complementary Mössbauer analysis.

4.2 Preparations

A rock saw was used if required for fitting the samples into the SEM-EDS sample chamber. Samples were mounted on a sample stub for the SEM-EDS analyses.

Fracture filling material for Mössbauer and geochemical analysis was scraped of the fracture surface using a steel chisel.

4.3 Analytical work

4.3.1 SEM-EDS

The fracture surfaces were examined by scanning electron microscopy at the University of Gothenburg, Sweden. The microscope is a Hitachi S-3400N scanning electron microscope (SEM) equipped with an INCADryCool energy dispersive X-Ray spectrometer (EDS). The instrument was operated using low-vacuum mode (15 Pa). Mineral identification was carried out using EDS-spectrums and quantitative mineral analyses.

4.3.2 Mössbauer spectroscopy

Mössbauer measurements were carried out by Henrik Skogby at the Department of Mineralogy, Swedish Museum of Natural History, Stockholm. Measurements were performed on powdered sample material carefully mixed and grounded with a transoptic resin, before heated (130°C) and pressed into a thin disc. For all samples, the amount of material (15–107 mg) was chosen according to the thin absorber approximation. Mössbauer spectra were acquired at room temperature using a conventional spectrometer system (Wissel) operated in constant acceleration mode with a nominal

50 mCi ^{57}Co/Rh source, and with the absorber held at an angle of 54.7° to the γ-rays to avoid orientation effects. Spectral data were recorded for the velocity range –11 to +11 mm/s in a multichannel analyser using 1024 channels. After velocity calibration against α-iron foil spectra, raw spectrum data were folded and fitted using a least square fitting program (Jernberg and Sundqvist 1983). Lorentzian lines, equal recoil free fractions, and equal intensity of the quadrupole components were assumed in the fitting procedure. For the magnetic spectra, the intensity ratios among the individual peaks were constrained to a 3:2:1-relationship. The spectra were normally fitted with one absorption doublet for Fe^{2+} in silicates, two doublets for Fe^{3+} in silicates, and one magnetic sextet. The detection limit is 2–3% of the total Fe content.

4.3.3 ICP-AES/ICP-QMS

ICP-AES/ICP-QMS analyses were carried out by ALS Scandinavia AB in Luleå, Sweden. The samples were fused with $LiBO_2$ and dissolved in dilute HNO_3. LOI (loss on ignition) is carried out at 1,000°C. Analyses are carried out according to EPA methods (modified) 200.7 (ICP-AES) and 200.8 (ICP-QMS).

5 Results

5.1 Iron hydroxide-bearing fractures in Sicada

All fractures in drill cores KFR102B, KFR103, KFR104 and KFR106 mapped as iron hydroxide-bearing during the coremapping and reported to Sicada are listed in Table 5-2.

In total, 61 fractures from the selected drill cores were mapped as iron hydroxide-bearing in Sicada. The majority of these (53) were found in KFR104 whereas no iron hydroxide occurrences were recorded in KFR103 (Table 5-1).

Upon visual inspection of the drill cores, 30 fractures were excluded for further analysis since the presence of iron hydroxide could be excluded visually (Table 5-1). Three additional fractures were not sampled since adjacent identical fractures were sampled and two fractures had already been sampled during a study of uranium mineralisations in KFR106 (Sandström et al. 2011). 26 fractures mapped as iron hydroxide-bearing were selected and sampled for SEM-EDS analysis. Detailed descriptions of these are presented in Appendix 1.

In all but two of the sampled fractures, it could be concluded based on the SEM-EDS analyses that the often rust-brown minerals assigned as iron-hydroxide in Sicada were in fact other minerals:

- The most common rust-coloured mineral mistaken for iron hydroxide during the drill core mapping is Fe-rich mixed layer clay (Figure 5-1). (10 of 26 fractures mapped as iron hydroxide-bearing.)
- A significant number of fractures mapped as iron hydroxide-bearing with a brown or green-yellow coating were actually coated with U-silicate, U-oxide or U-phosphate (Figure 5-2). (7 of 26 fractures mapped as iron hydroxide-bearing.)
- A few of the fractures mapped as iron hydroxide-bearing contained rust-coloured metallic iron or iron oxides from the drilling process (Figure 5-3). (4 of 26 fractures mapped as iron hydroxide-bearing.)
- Other minerals mistaken for iron hydroxide during the drill core mapping include hematite-stained adularia and albite. (3 of 26 fractures mapped as iron hydroxide-bearing.)

Only two of the sampled fractures mapped as iron hydroxide-bearing in Sicada were actually coated with a mineral which possibly can be iron hydroxide (Table 5-3). The elevations of the two samples are –45.06 m and –78.03 m.

Table 5-1. Iron hydroxide occurrences in Sicada based on the drill core mapping of KFR102B, KFR103, KFR104 and KFR106.

	Number of fractures mapped as iron hydroxide in Sicada	Number of fractures inferred to possibly contain iron hydroxide after visual inspection	Number of fractures inferred to possibly contain iron hydroxide after SEM-EDS analysis
KFR102B	4	3	0
KFR103	0	0	0
KFR104	53	24	2
KFR106	4	4	0

Photo of fracture surface with rust-brown colour.

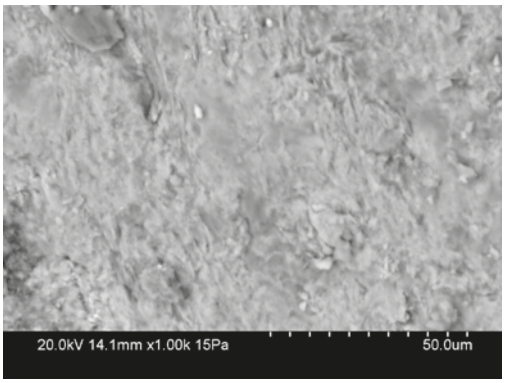

Backscattered electron image of mixed layer clay on fracture surface.

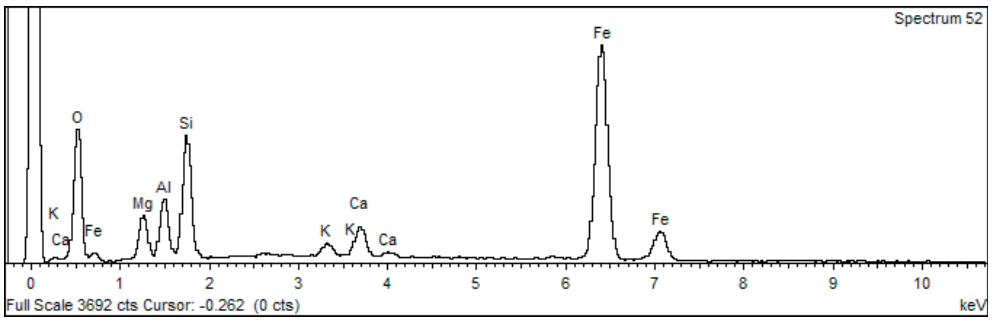

EDS-spectra of Fe-rich mixed layer clay.

Figure 5-1. *Fracture from KFR104 25.03–25.09 m. The rust-brown mineral mapped as iron hydroxide in Sicada is a Fe-rich mixed layer clay.*

Photo of fracture surface green-yellow mineral coating.

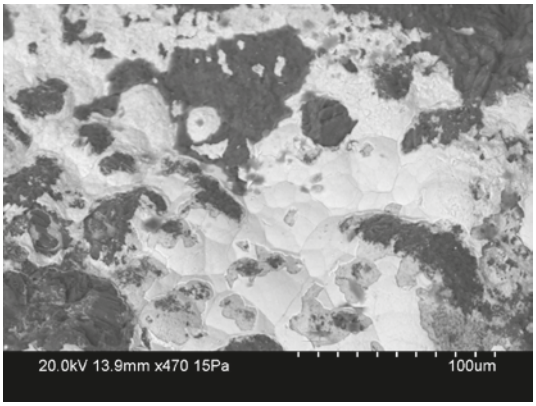

Backscattered electron image of U,Ca-oxide on fracture surface.

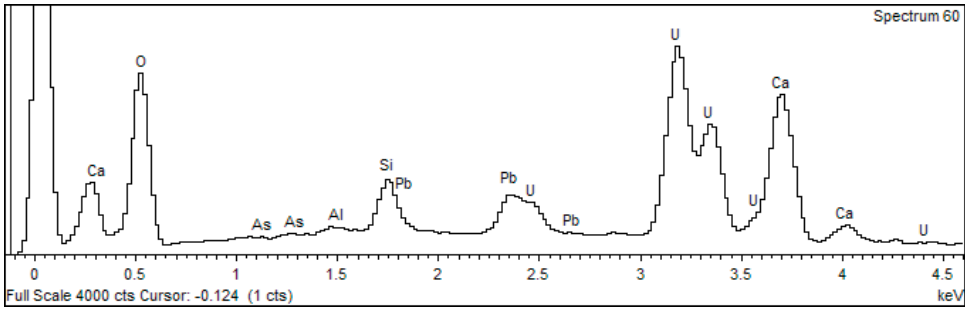

EDS-spectra of U,Ca-oxide.

Figure 5-2. *Fracture from KFR104 21.57–21.66 m. The green-yellow mineral mapped as iron hydroxide in Sicada is an (U,Ca)-oxide.*

Photo of fracture surface with rust-brown mineral coating.

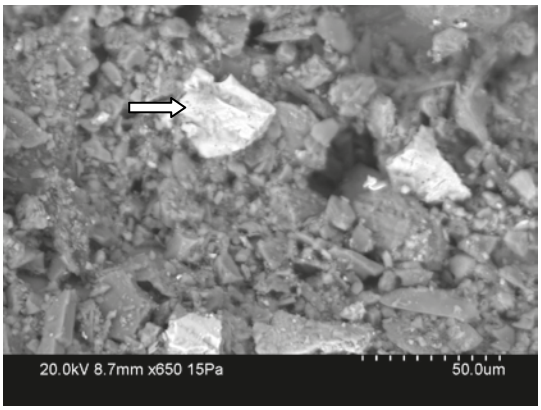

Backscattered electron image of fragments of metallic iron on the fracture surface.

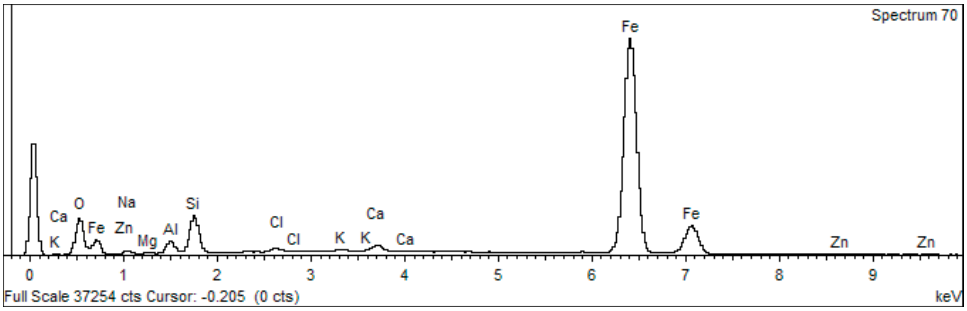

EDS-spectra of metallic iron.

Figure 5-3. *Fracture from KFR102B 113.56–113.88 m. The rust-brown coating mapped as iron hydroxide in Sicada consists of fragments of metallic iron from the drilling process.*

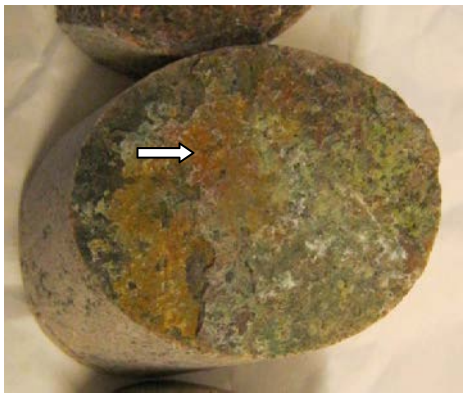

Photo of fracture surface with rust-brown mineral coating.

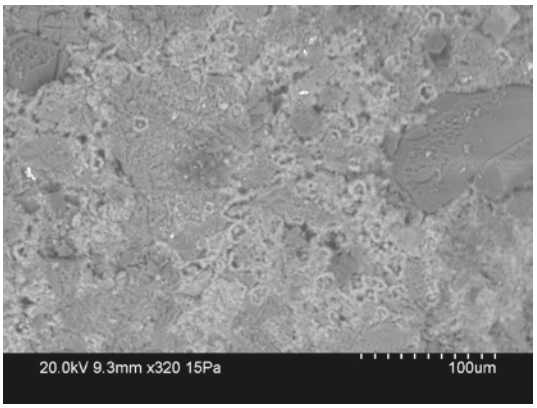

Backscattered electron image of potential iron hydroxide.

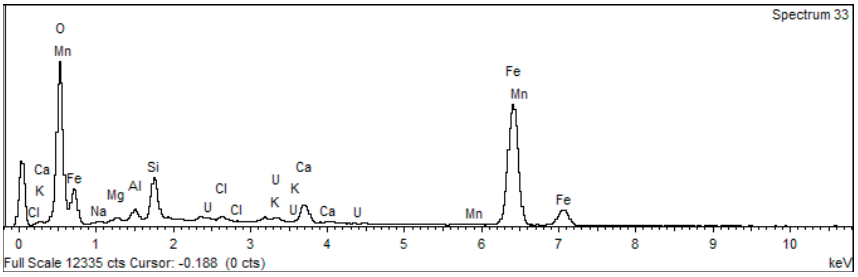

EDS-spectra of iron hydroxide.

Figure 5-4. *Fracture from KFR104 99.32–99.42 m. The rust-brown precipitate may be iron hydroxide.*

Table 5-2. All iron hydroxide occurrences in Sicada based on the drill core mapping in KFR102B, KFR103, KFR104 and KFR106.

Idcode	Adjusted secup	Elevation Adjusted secup	Min1	Min2	Min3	Min4	Not sampled	Comment	Sample name*
KFR102B	17.173	–11.50	Laumontite	Chlorite	Calcite	Iron Hydroxide	X	Hm-stained Laumontite	
KFR102B	17.452	–11.73	Chlorite	Iron Hydroxide	Laumontite	Quartz			17.45–17.49
KFR102B	26.826	–19.34	Chlorite	Iron Hydroxide	Oxidized Walls				26.76–26.91
KFR102B	113.720	–89.61	Chlorite	Calcite	Iron Hydroxide				113.56–113.88
KFR104	21.504	–14.77	Chlorite	Iron Hydroxide	Calcite				21.44–21.52
KFR104	21.628	–14.88	Chlorite	Calcite	Muscovite	Iron Hydroxide			21.57–21.66
KFR104	25.062	–17.68	Chlorite	Calcite	Iron Hydroxide	Hematite			25.03–25.09
KFR104	25.568	–18.10	Chlorite	Calcite	Iron Hydroxide				25.51–25.62
KFR104	26.885	–19.17	Chlorite	Calcite	Iron Hydroxide		X	Sulphides, same as 27.04	
KFR104	27.085	–19.34	Chlorite	Muscovite	Iron Hydroxide				27.04–27.11
KFR104	29.894	–21.63	Chlorite	Calcite	Iron Hydroxide	Hematite			29.80–29.93
KFR104	30.241	–21.91	Chlorite	Iron Hydroxide	Laumontite				30.20–30.28
KFR104	32.677	–23.90	Chlorite	Calcite	Iron Hydroxide				32.67–32.76
KFR104	35.495	–26.20	Laumontite	Hematite	Iron Hydroxide	Calcite	X	Hm-stained Laumontite	
KFR104	43.614	–32.82	Chlorite	Calcite	Laumontite	Iron Hydroxide			43.53–43.76
KFR104	55.407	–42.41	Chlorite	Calcite	Iron Hydroxide		X	Hm-stained clay mineral	
KFR104	55.968	–42.87	Chlorite	Calcite	Iron Hydroxide				55.95–56.04
KFR104	59.280	–45.56	Iron Hydroxide						59.21–59.25
KFR104	59.729	–45.92	Chlorite	Calcite	Iron Hydroxide	Muscovite			59.71–59.75
KFR104	99.402	–78.03	Chlorite	Calcite	Iron Hydroxide	Epidote			99.32–99.42
KFR104	109.420	–86.08	Chlorite	Clay Minerals	Iron Hydroxide		X	Hm-stained clay mineral	
KFR104	110.521	–86.97	Chlorite	Iron Hydroxide			X	Brown mineral in pegmatite	
KFR104	122.204	–96.31	Chlorite	Calcite	Iron Hydroxide	Laumontite	X	No FeOOH	
KFR104	122.531	–96.57	Iron Hydroxide						122.52–122.56
KFR104	126.697	–99.90	Calcite	Chlorite	Iron Hydroxide		X	No FeOOH	
KFR104	129.253	–101.94	Chlorite	Calcite	Iron Hydroxide		X	Hm-stained adularia	
KFR104	129.311	–101.98	Chlorite	Calcite	Iron Hydroxide		X	Hm-stained adularia	
KFR104	134.719	–106.30	Iron Hydroxide						134.70–134.75
KFR104	139.195	–109.86	Chlorite	Iron Hydroxide			X	Hm-stained clay mineral	
KFR104	152.656	–120.57	Calcite	Chlorite	Iron Hydroxide		X	Hm-stained clay mineral	

KFR104	268.249	–210.98	Chlorite	Calcite	Iron Hydroxide		X	Hm-stained laumontite	
KFR104	268.852	–211.45	Chlorite	Calcite	Iron Hydroxide	Laumontite	X	Hm-stained laumontite	
KFR104	270.168	–212.46	Chlorite	Clay Minerals	Iron Hydroxide				270.17–270.23
KFR104	279.645	–219.76	Chlorite	Calcite	Iron Hydroxide	Laumontite	X	Hm-stained chlorite/laumontite	
KFR104	280.540	–220.45	Chlorite	Epidote	Iron Hydroxide				280.54–280–61
KFR104	280.927	–220.75	Chlorite	Clay Minerals	Hematite	Iron Hydroxide	X	Hm-stained adularia+laumontite	
KFR104	283.412	–222.66	Chlorite	Calcite	Hematite	Iron Hydroxide	X	Hm-stained adularia+laumontite	
KFR104	283.738	–222.91	Calcite	Laumontite	Iron Hydroxide	Hematite	X	Hm-stained adularia+laumontite	
KFR104	284.087	–223.18	Chlorite	Hematite	Calcite	Iron Hydroxide	X	Hm-stained adularia+laumontite	
KFR104	286.020	–224.66	Laumontite	Iron Hydroxide	Muscovite		X	Hm-stained adularia+laumontite	
KFR104	288.808	–226.81	Chlorite	Calcite	Hematite	Iron Hydroxide	X	Hm-stained adularia+laumontite	
KFR104	290.893	–228.41	Clay Minerals	Calcite	Iron Hydroxide		X	Hm-stained adularia+laumontite	
KFR104	291.300	–228.72	Chlorite	Laumontite	Hematite	Iron Hydroxide	X	Hm-stained adularia+laumontite	
KFR104	293.460	–230.38	Calcite	Hematite	Iron Hydroxide		X	Same as 293.461	
KFR104	293.461	–230.38	Clay Minerals	Chlorite	Iron Hydroxide				293.23–293.29
KFR104	293.511	–230.42	Chlorite	Calcite	Hematite	Iron Hydroxide	X	Same as 293.461	
KFR104	294.067	–230.84	Calcite	Chlorite	Hematite	Iron Hydroxide			294.02–294.15
KFR104	296.668	–232.84	Calcite	Iron Hydroxide	Hematite	Chlorite	X	No FeOOH	
KFR104	303.760	–238.27	Chlorite	Calcite	Iron Hydroxide		X	Pegmatite mineral	
KFR104	306.748	–240.56	Chlorite	Hematite	Calcite	Iron Hydroxide	X	Hm stained chlorite	
KFR104	326.806	–255.89	Clay Minerals	Iron Hydroxide	Chlorite	Oxidized Walls	X	Clay mineral	
KFR104	327.408	–256.35	Iron Hydroxide				X	Clay mineral	
KFR104	328.796	–257.41	Calcite	Chlorite	Iron Hydroxide	Adularia			328.75–328.86
KFR104	390.013	–303.65	Chlorite	Iron Hydroxide					389.97–390.03
KFR104	416.790	–323.66	Chlorite	Calcite	Iron Hydroxide	X2			416.96–416.35
KFR104	417.412	–324.12	Calcite	Iron Hydroxide			X	Hm-stained adularia	
KFR104	418.401	–324.86	Calcite	Clay Minerals	Chlorite	Iron Hydroxide	X	Hm-stained adularia	
KFR106	9.750	–8.12	Calcite	Chlorite	Iron Hydroxide				9.72–9.77
KFR106	85.308	–79.03	Clay Minerals	Chlorite	Calcite	Iron Hydroxide	X	Already sampled (P-11-41)	
KFR106	155.995	–145.20	Clay Minerals	Iron Hydroxide			X	No FeOOH	
KFR106	262.574	–244.76	Clay Minerals	Iron Hydroxide			X	Already sampled (P-11-41)	

* Sample name: Name of the drill core sample, see Appendix 1.

Table 5-3. Fracture mineralogy of the samples investigated by SEM-EDS.

Drill core	Sample (m)	Clay mineral	Chlorite	Quartz	Adularia	Albite	Calcite	Pyrite	Barite	U-mineral	Hematite	Fe-hydroxide	Other
KFR102B	17.45	X											Prehnite, Monazite
KFR102B	26.76	X			X		X						
KFR102B	113.56	X		X		X							Metallic Fe
KFR104	21.44	X								X(si)			
KFR104	21.57	X							X	X(si)			
KFR104	24.80*						X			X(p)	X		
KFR104	25.03	X			X					X(si)			
KFR104	25.51	X							X	X(si)			Galena, monazite
KFR104	27.04	X											
KFR104	29.80	X			X				X	X(p)			
KFR104	30.20	X	X								X		Laumontite
KFR104	32.67	X								X(p)			
KFR104	43.53	X			X	X					X		Ca(REE)-carbonate
KFR104	55.95	X											
KFR104	59.21									X(si)	X	X	
KFR104	59.71	X					X						Metallic Fe
KFR104	61.55*	X					X	X					Galena, sphalerite, Zn oxide
KFR104	99.32	X								X(si)		X	Laumontite, Ca(REE)-carbonate
KFR104	107.64*	X											Laumontite
KFR104	122.52							X					Drilling debris
KFR104	134.70				X		X						Laumontite
KFR104	270.17	X			X						X		Prehnite
KFR104	280.54	X									X		Laumontite
KFR104	293.23	X											Fe oxide
KFR104	294.02	X			X	X		X			X		
KFR104	328.75	X								X(si)			
KFR104	389.97	X			X			X		X(si)			Metallic Fe
KFR104	416.96	X											Galena
KFR106	9.72	X									X		

*Samples selected for Mössbauer analysis; not Fe-hydroxide bearing in Sicada.

5.2 Geochemical analyses

The obtained geochemical data of bulk fracture filling material are presented in Table 5-4.

Table 5-4. Geochemistry of bulk fracture filling material.

	KFR102B 113.56 m	KFR104 13.22 m	KFR104 25.51 m	KFR104 43.53 m	KFR104 61.55 m	KFR104 107.64 m	KFR104 276.60 m	KFR104 416.96 m
SiO_2 (wt%)	48.7	51.2	40.0	36.1	16.2	35.1	71.8	45.6
Al_2O_3	13.1	18.7	13.3	12.4	3.81	13.8	14.4	18.1
CaO	10.2	4.88	3.24	22.4	38.3	26.6	2.13	8.35
Fe_2O_3	6.31	7.70	22.2	5.78	5.18	1.90	4.33	9.77
K_2O	5.73	4.07	2.67	4.63	1.01	1.69	4.60	4.23
MgO	5.71	3.86	4.25	1.34	1.06	0.317	1.27	2.60
MnO	0.0923	0.0832	0.0659	0.0845	0.0579	0.0361	0.0761	0.0492
Na_2O	0.931	2.24	1.37	1.06	0.256	0.23	1.69	0.24
P_2O_5	0.0198	0.0506	< 0.006	0.0042	0.0136	< 0.002	0.0634	< 0.009
TiO_2	0.0754	0.109	0.0172	0.0118	0.0525	0.0089	0.241	0.0168
Sum	90.9	92.9	87.1	83.8	65.9	79.7	100.6	89.0
LOI	n.a.	n.a.	n.a.	n.a.	n.a.	n.a.	n.a.	n.a.
Ba (mg/kg)	557	1110	1820	338	155	958	588	116
Be	3.28	3.99	6.51	6.42	1.23	2.89	3.4	12.1
Co	15	< 40	< 10	< 6	< 6	16.2	6.67	< 5
Cr	22.3	85.3	< 30	< 10	14.5	< 10	89.3	16.4
Cs	0.62	1.97	32.2	17.6	0.704	4.55	4.25	39.8
Ga	16.6	21.2	16.6	18.3	4.36	21.5	18.4	30.5
Hf	1.25	4.89	2.55	4.47	0.621	0.118	3.6	0.164
Mo	< 3	54.1	< 6	< 2	< 2	< 2	< 5	< 5
Nb	6.55	16.3	3.72	3.25	3.77	2.39	10.5	< 5
Ni	< 20	< 80	< 30	< 10	< 10	< 10	32.4	< 10
Rb	81.8	97.5	118	152	41.9	80	168	336
Sc	10.4	< 8	< 3	< 1	2.13	< 1	15.6	2.93
Sr	214	94.5	129	58.7	54.9	152	178	107
Ta	1.04	0.712	0.357	0.456	0.183	0.209	2.52	0.0702
Th	10.1	9.00	5.71	7.06	1.98	0.613	8.48	0.493
U	7.98	8.67	2170	57.9	5.07	483	11.1	9.4
V	74.6	< 20	< 6	21.8	2.88	< 2	35.1	28.1
W	0.541	< 2	16.1	0.81	1.33	3.63	< 50	< 50
Y	42.8	40.7	191	143	97.2	75.2	33.6	101
Zr	35.2	137	170	75.3	24.5	< 2	112	6.59
La	438	24.8	27.9	22.8	29.5	30.7	62.7	23.7
Ce	649	55.6	136	48.8	85.8	56.2	100	49.3
Pr	68.9	< 8	11.8	5.69	13.0	8.34	12.8	6.5
Nd	205	18.2	44.1	19.1	52.9	28.8	43.5	27.2
Sm	20.4	4.1	17.3	7.77	11.9	8.9	7.55	10.7
Eu	1.33	0.761	2.99	2.35	2.61	1.64	1.44	1.58
Gd	11.6	5.02	25.3	13	15.5	10.4	5.96	14.7
Tb	1.67	1.10	5.30	3.24	1.96	2.17	0.97	2.91
Dy	8.37	5.9	33.9	22.5	9.98	13.6	5.72	18.5
Ho	1.73	1.5	8.79	5.84	2.23	3.22	1.34	4.05
Er	4.3	4.48	26.5	17.4	5.54	9.03	4.08	11.8
Tm	0.566	< 0.8	4.18	2.78	0.742	1.33	0.621	1.71
Yb	3.44	4.31	25.9	18.1	4.52	7.75	4.28	11.6
Lu	0.592	0.813	4.57	3.25	0.824	1.30	0.70	1.93

5.3 Mössbauer analyses

The results from the Mössbauer analyses are presented in Table 5-5. No correlation between depth and oxidation factor can be seen in the data (Figure 5-5). In two samples of the samples, the amount of Fe(II) were below the detection limit.

No precautions were taken to avoid oxidation during storage and sampling of the drill cores and it cannot be excluded that some oxidation of the fracture surfaces has occurred after the drill cores were obtained from the boreholes. Therefore, the obtained Mössbauer data represent maximum values of the degree of oxidation of the fracture surface. For the safety assessment, this is conservative since the oxidation capacity may be underestimated in the obtained data. The drill cores from the Forsmark PLU were handled in the same manner and the relative differences seen between the Mössbauer data from the Forsmark PLU and SFR are considered significant.

Table 5-5. Results from the Mössbauer analyses. Fe_2O_3(tot)-content of the corresponding fracture fillings based on ICP-AES analysis also presented in the table.

Sample	Elevation (m.a.s.l.)	Fe_2O_3(tot) (wt%)	Fe(II)/Fe(tot)	Oxidation factor Fe(III)/Fe(tot)
KFR01 45.18 m	–87.11	7.77	0.76	0.24
KFR7A 70.05 m	–134.73	2.24	0.26	0.74
KFR19 90.56 m	–59.1	4.07	0.00	1.00
KFR105 126.9 m	–128.37	8.33	0.57	0.43
KFR105 283.38 m	–153.22	33.1	0.25	0.75
KFR102B 113.56 m	–89.61	6.31	0.71	0.29
KFR104 13.22 m	–8.05	7.70	0.81	0.19
KFR104 25.51 m	–18.10	22.2	0.13	0.87
KFR104 43.53 m	–32.82	5.78	0.79	0.21
KFR104 61.55 m	–47.54	5.18	0.51	0.49
KFR104 107.64 m	–84.72	1.90	0.00	1.00
KFR104 276.60 m	–217.57	4.33	0.34	0.66
KFR104 416.96 m	–323.66	9.77	0.64	0.36

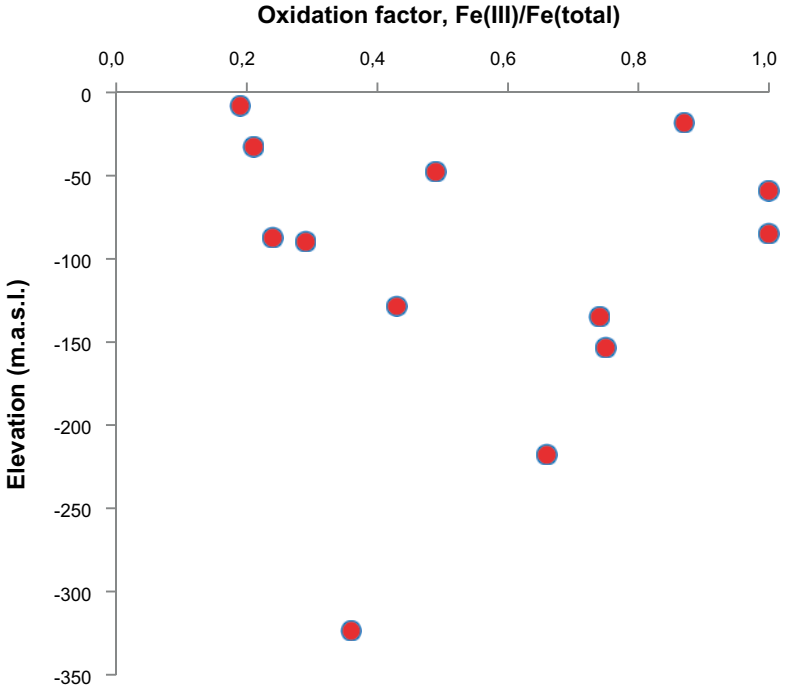

Figure 5-5. *Total oxidation factor of bulk fracture filling material versus elevation.*

6 Statistical analysis of ferrous iron abundance in fracture minerals at SFR

6.1 Description of data used in analysis

In this section, sampled data are statistically analysed and parameterised to facilitate the use of the fracture mineral iron content in subsequent modelling. No attempt has been made to couple process understanding to the sampled data, and exhaustive interpretations have been avoided. Instead, the resulting distributions should be considered as estimations roughly describing the presumable range of iron contents in fracture minerals at SFR.

The samples used in this statistical analysis are listed in Table 6-1 along with the results from ICP-AES (Fe_2O_3(tot)) and Mössbauer (Fe(II)/Fe(tot)) analyses. For samples where results for both total iron and Fe(II)/Fe(tot) analyses exists, the Fe(II) content is calculated according to Eqn. 6-1 and compared with the derived distribution.

$$\mathrm{wt\%}\left(\mathrm{Fe(II)}\right) = \frac{2M_{\mathrm{Fe}}}{M_{\mathrm{Fe_2O_2}}} \cdot \mathrm{wt\%}\left(\mathrm{Fe_2O_3}\right) \cdot \mathrm{wt\%}\left(\mathrm{Fe(II)/Fe(tot)}\right) \qquad \text{Eqn. 6-1}$$

Table 6-1. Samples used in the analysis.

Sample	Elevation (m.a.s.l)	Fe_2O_3 (wt%)	Fe(II)/Fe(tot)	Fe(II) (wt%)	Main Fe-mineral
KFR01 45.18	–87.11	7.77	0.76	5.91	Clay mineral
KFR01 47.09	–88.76	1.16			Clay mineral
KFR7A 49.60	–134.02	7.21			Clay mineral, Fe hydroxide
KFR7A 68.80	–134.69	0.89			Clay mineral
KFR7A 70.05	–134.73	2.24	0.26	0.58	Clay mineral
KFR7A 70.47	–134.75	0.307			No Fe mineral identified
KFR08 76.77	–92.71	2.35			Clay mineral
KFR08 95.29	–94.33	3.15			Clay mineral, hematite
KFR10 95.65	–145.94	15.8			Chlorite, biotite, hematite
KFR10 106.3	–153.47	7.25			Clay mineral
KFR19 90.56	–59.10	4.07	0*	0*	Hematite, clay mineral
KFR105 126.9	–128.37	8.33	0.57	4.75	Clay mineral, chlorite
KFR105 280.07	–152.72	0.832			Small amounts of biotite
KFR105 283.38	–153.22	33.1	0.25	8.28	Clay mineral
KFR102B 113.56	–89.61	6.31	0.71	4.48	Clay mineral
KFR104 13.22	–8.05	7.70	0.81	6.24	Clay mineral
KFR104 25.51	–18.10	22.2	0.13	2.89	Clay mineral
KFR104 43.53	–32.82	5.78	0.79	4.57	Clay mineral
KFR104 61.55	–47.54	5.18	0.51	2.64	Clay mineral
KFR104 107.64	–84.72	1.90	0*	0*	Laumontite, clay mineral
KFR104 276.60	–217.57	4.33	0.34	1.47	Clay mineral
KFR104 416.96	–323.66	9.77	0.64	6.25	Clay mineral

*Totally oxidised sample. Half-detection limit (1.5 wt%) is used in calculations.

6.2 Estimation of the distribution of total iron content

The total fracture mineral iron content is analysed by means of ICP-AES and the result is expressed as the equivalent weight fraction of Fe_2O_3 in the samples. These sampled weight fractions of Fe_2O_3 were analysed statistically and a fitted beta distribution was found to fairly well comprise the sampled data distribution (Figure 6-1). Assuming that the total iron content is beta distributed the population median content of Fe_2O_3 is approximately 4.5 wt% with a standard deviation of ~7.7.

6.3 Estimation of the distribution of the oxidation factor

The oxidation state of the iron samples is analysed by means of Mössbauer analyses. The sampled Fe(II)/Fe(tot) ratios were analysed statistically and also found to be fairly well described by a beta distribution (Figure 6-2).

Assuming that the oxidation factors are beta distributed, the population median Fe(II)/Fe(tot) ratio is approximately 0.42 with a standard deviation of ~0.29.

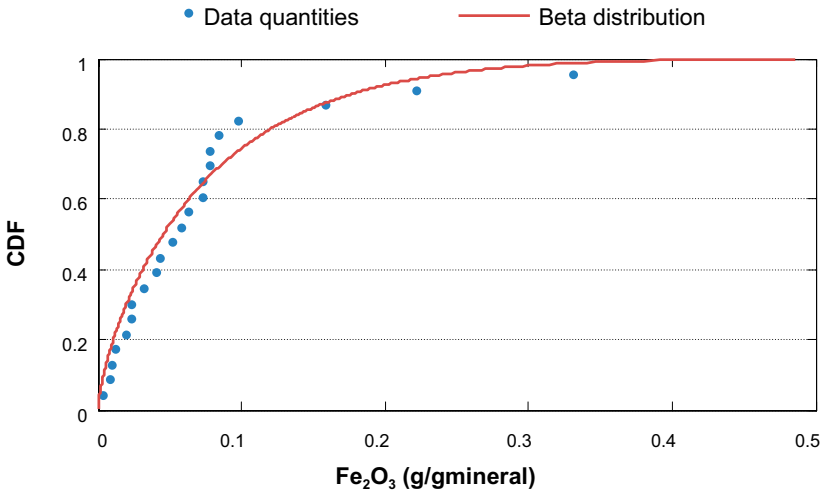

Figure 6-1. *Total iron content for the SFR samples (expressed in terms of Fe_2O_3(tot)) and a fitted beta distribution with parameters α = 0.72 and β = 9.36 with population median(std) = 0.045(0.077) $g/g_{mineral}$. CDF = cumulative distribution function.*

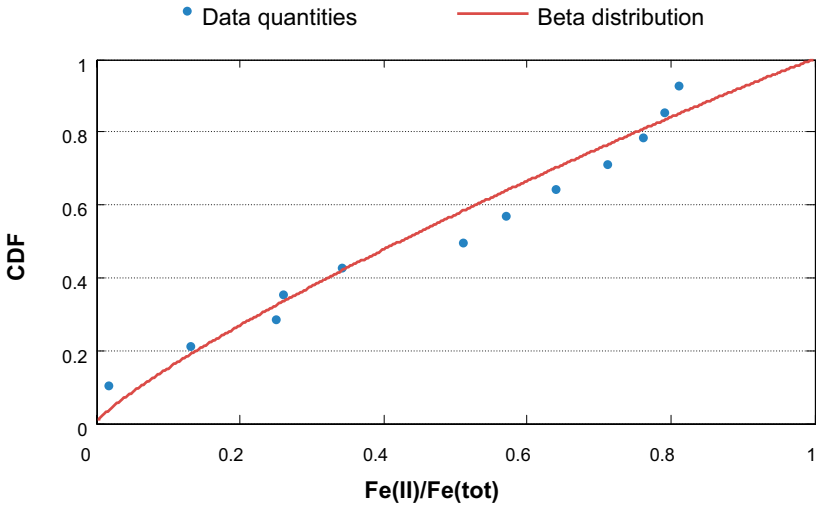

Figure 6-2. *Fe(II)/Fe(tot) mass ratio from Mössbauer analysis of SFR samples, and a fitted beta distribution with parameters α = 0.84 and β = 1.04 (population median (std) = 0.424 (0.293)). CDF = cumulative distribution function.*

6.4 Calculation of Fe(II) content

The mass fraction of Fe(II) is calculated assuming that the total iron and oxidation factor are both beta distributed variables and that the oxidation factor is independent on the total iron content. A distribution of the fracture mineral Fe(II) content is calculated by Eqn. 6-1 using 100,000 values of Fe_2O_3 and Fe(II)/Fe(tot) stochastically sampled from their distributions. The resulting Fe(II) mass fraction distribution is shown in Figure 6-3.

Assuming that the amounts of Fe(II) in fracture minerals are beta distributed, the population median of the Fe(II) mass fraction is approximately 1.0 wt% with a standard deviation of ~3.2.

A statistical analysis of mineral abundances has previously been carried out on data from fracture mineral mapping at Forsmark (Löfgren and Sidborn 2010). A similar mapping has not been performed on samples from SFR. Although being a source of uncertainty, the results from the Forsmark analysis are used in the following to roughly estimate presumable specific amounts of ferrous iron in coatings along flowing fractures in SFR. Since more fracture filling material is present within fracture zones, and more fracture zones are encountered in the SFR drill cores (Curtis et al. 2011), it is considered conservative to use the data from Forsmark also for the SFR area in the sense that the risk for over-estimating the oxidation capacity is minimised.

At Forsmark, it was found that the averaged Fe(II)-bearing fracture mineral thicknesses d_{mean} (m) could well be represented by log-normal distribution and that the variation between different rock domains was small. The population parameters recommended in Löfgren and Sidborn (2010) for use in modelling are listed in Table 6-2.

Table 6-2. Averaged fracture mineral thickness d_{mean} (m) for Fe(II)-bearing fracture minerals where these factors could be quantitatively estimated (f_{quant}% of the mapped fractures). Modified from Löfgren and Sidborn (2010).

Mineral	$\bar{d}_{mean}$ (m)	μ of ln d_{mean}	σ of ln d_{mean}	f_{quant} (%)
Chlorite	$206 \cdot 10^{-6}$	–9.05	1.06	24
Clay minerals	$135 \cdot 10^{-6}$	–9.42	1.01	11
Pyrite	$6 \cdot 10^{-6}$	–16.14	2.90	10

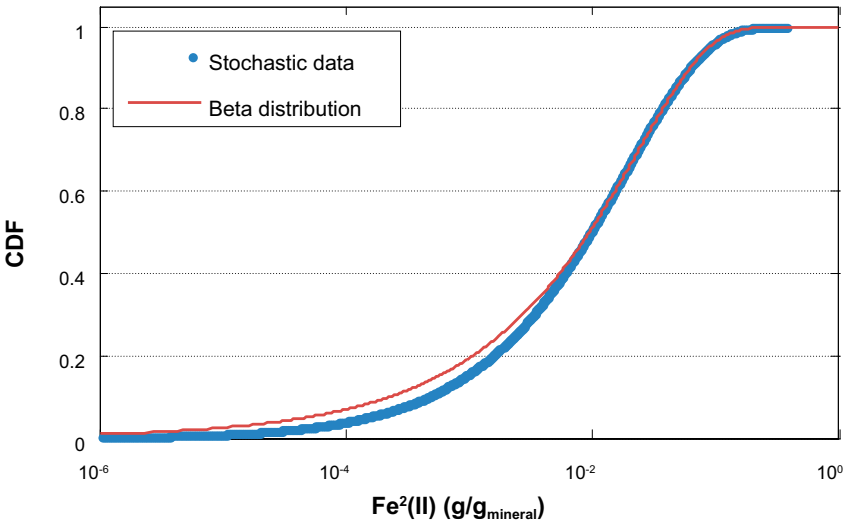

Figure 6-3. Stochastic Fe(II) mass fraction results, and a fitted beta distribution with parameters α = 0.45 and β = 19.59 (population median (std) = 0.010 (0.032) $g/g_{mineral}$). CDF = cumulative distribution function.

Here we assume that all Fe(II) is present in the fracture mineral chlorite. The mineral mapped as chlorite often consists of different proportions of chlorite and mixed layer clays. However, Fe(II) in the poorly crystallised clay minerals is more available than in chlorite and the simplified assumption is therefore considered conservative in the sense that the accessibility of Fe(II) is likely underestimated. The specific amount of Fe(II) (g/m^2) is calculated by Eqn. 6-2 using 100,000 values of d_{mean} (m) for chlorite and Fe(II) (g/g) stochastically sampled from their distributions.

$$\text{Fe(II)}\ (g/m^2) = \rho_{chlorite} \cdot d_{mean} \cdot \text{Fe(II)}\ (g/g) \qquad \text{Eqn. 6-2}$$

The resulting distribution for specific amount of Fe(II) along flowing fractures is shown in Figure 6-4. The density of chlorite $\rho_{chlorite}$ is taken to be 3×10^6 g/m^3 (Deer et al. 1999).

Assuming that the specific amounts of Fe(II) are log-normally distributed, the population median of specific ferrous iron along flowing fractures is estimated to 2.4 g/m^2 and the most abundant value (mode) would be ~0.01 g/m^2. Note that the mineral thickness d_{mean} and fracture mineral ferrous iron content Fe(II) ($g/g_{chlorite}$) are assumed to be uncorrelated in this calculation.

The distributions calculated for SFR can be compared with results calculated for Forsmark samples. The Forsmark data have previously been calculated and used in Sidborn et al. (2010) assuming log-normally distributed total iron concentrations and oxidation factors. However, these data are here re-evaluated assuming beta distributed Fe_2O_3(tot) and Fe(II)/Fe(tot) data to facilitate comparison between the sites. The comparison is shown in Figure 6-5 for ferrous iron (g/g) content in fracture minerals) and Figure 6-6 for specific ferrous iron content (g/m^2) along flow paths.

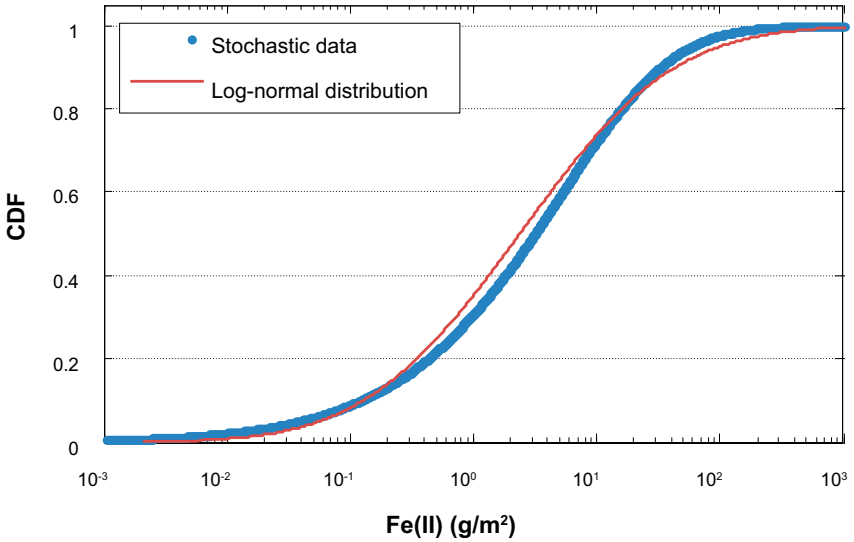

Figure 6-4. *Stochastic results of specific amounts of Fe(II) along flowing fractures. Stochastic results are shown along with a fitted log-normal distribution with parameters μ_e = 0.86 and σ_e = 2.27 (population median (std) = 2.37 (415) g/m^2). CDF = cumulative distribution function.*

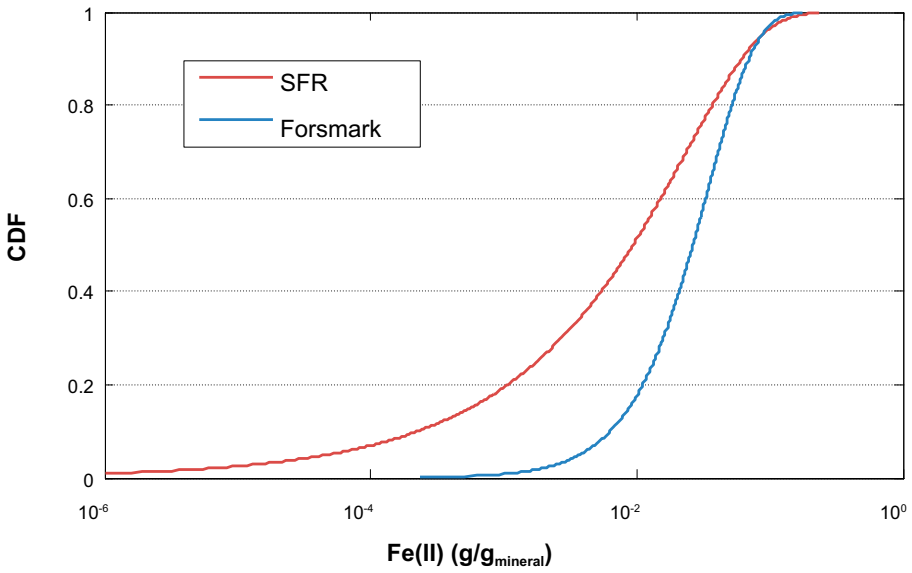

Figure 6-5. *Calculated beta distributions of Fe(II) content in fracture minerals in SFR (α = 0.45 and β = 19.59) in comparison with re-evaluated Forsmark data used in Sidborn et al. (2010) (α = 1.44 and β = 41.64). CDF = cumulative distribution function.*

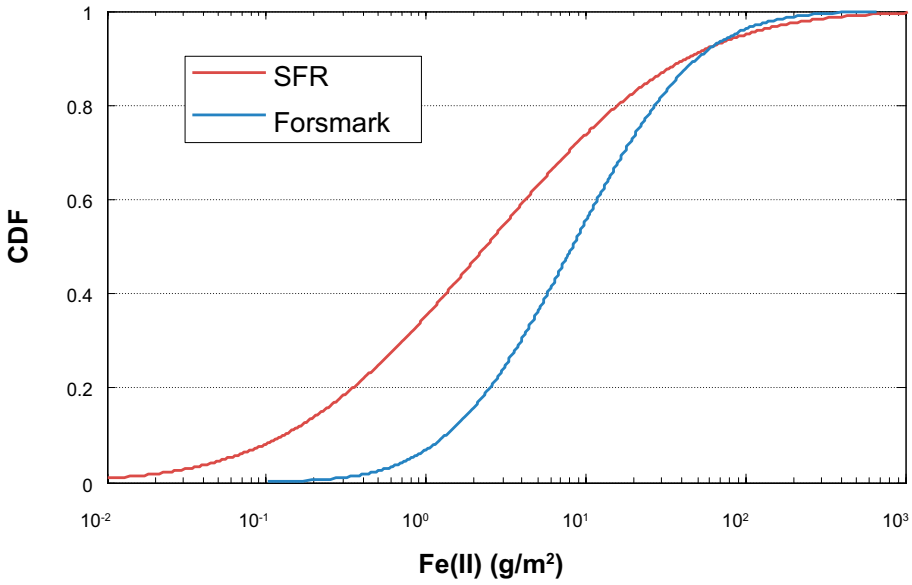

Figure 6-6. *Calculated log-normal distributions of specific Fe(II) content along flowing fractures in SFR (μ_e = 0.86 and σ_e = 2.27) in comparison with re-evaluated Forsmark data used in Sidborn et al. (2010) (μ_e = 2.11 and σ_e = 1.42). CDF = cumulative distribution function.*

7 Concluding remarks

In the investigated drill cores KFR102B, KFR103, KFR104 and KFR106, a total number of 61 fractures in Sicada had been mapped as iron hydroxide-bearing during the drill core mapping. A detailed investigation of these fractures shows that all but two can be dismissed as iron hydroxide-bearing. The two samples potentially iron hydroxide-bearing are both found in KFR104 and occur at elevations –45.56 and –78.03 m.a.s.l., respectively. None of the modelled deformation zones (DZ) is closer than 10 m from either one of the two samples (Curtis et al. 2011). Minerals mistaken for iron hydroxide during the drill core mapping are preferably Fe-rich clay mineral, but also uranium minerals, hematite stained adularia and albite, and metallic iron or iron oxides from the drilling process. Based on data from the drill core mapping, sulphides occur on fracture surfaces at most depths at SFR, the absence of sulphides in water conductive fractures in the upper 30 m could be due to intrusion of oxygenated waters during some period(s).

Based on the available data, the fracture filling material appears to be more oxidised at SFR compared at the Forsmark site. This could be due to the higher frequency of water conductive fracture zones in the SFR bedrock compared to the very dry bedrock at Forsmark (cf. SKB 2008, Öhman et al. 2012), enabling larger inflow of oxygenenated water at some period in the hydrogeological evolution of the area. Some of the oxidation of the fracture filling material may be of hydrothermal origin and thus > 1,000 Ma (cf. Sandström et al. 2008, 2009). The concentration of Fe(total) in the fracture filling material is lower at SFR, in agreement with the higher abundance of the mixed layer clay illite-smectite instead of corrensite which is the most common clay mineral found in fractures at the Forsmark site (Sandström and Tullborg 2011, Sandström et al. 2008). The combination of more oxidised fracture filling material and lower abundance of iron provide a lower amount of available Fe(II) in the fracture system at SFR compared to at the Forsmark site. Summaries of the results from the statistical analysis are presented in Table 7-1 and Table 7-2.

In order to obtain time constraints on the oxidation of the fracture filling material, uranium series measurements would be required (cf. Tullborg et al. 2008). This is currently carried out on fracture filling material from drill core KFR106 within the scope of the project “Uranium and redox conditions in Forsmark”, those data will also increase the understanding of the redox conditions at SFR.

Table 7-1. Summary of statistical results for calculated distributions of Fe_2O_3 abundance and Fe(II)/Fe(tot) mass ratio in fracture minerals in sampled boreholes in the SFR area.

	Beta distributed content in fracture minerals		
	α	β	median (std)
Fe_2O_3(total) ($g/g_{mineral}$)	0.72	9.36	0.045 (0.077)
Fe(II)/Fe(tot)	0.84	1.04	0.424 (0.293)

Table 7-2. Summary of statistical results for calculated distributions of Fe(II) abundance in fracture minerals in sampled boreholes in the SFR area. Forsmark data are included for comparison.

	Beta distributed Fe(II) content in fracture minerals			Log-normally distributed Fe(II) abundance per fracture surface		
Site	α	β	median (std) ($g/g_{mineral}$)	μ_e	σ_e	median (std) (g/m^2)
SFR	0.45	19.59	0.010 (0.032)	0.86	2.27	2.37 (415)
Forsmark	1.44	41.64	0.026 (0.027)	2.11	1.42	8.24 (57.2)

References

SKB's (Svensk Kärnbränslehantering AB) publications can be found at www.skb.se/publications.

Curtis P, Markström I, Petersson J, Triumf C-A, Isaksson H, Mattsson H, 2011. Site investigation SFR. Bedrock geology. SKB R-10-49, Svensk Kärnbränslehantering AB.

Deer W A, Howie R A, Zussman J, 1992. An introduction to the rock-forming minerals. 2nd ed. Harlow: Longman.

Drake H, Tullborg E-L, 2009. Oskarshamn site investigation. Investigation of goethite-bearing fractures in cored boreholes. Laxemar subarea. SKB P-09-15, Svensk Kärnbränslehantering AB.

Jernberg P, Sundqvist T, 1983. A versatile Mössbauer analysis program. Report UU-IP-1090, Institute of Physics, Uppsala University.

Löfgren M, Sidborn M, 2010. Statistical analysis of results from the quantitative mapping of fracture minerals in Forsmark. Site descriptive modelling – complementary studies. SKB R-09-30, Svensk Kärnbränslehantering AB.

Nilsson A-C, Tullborg E-L, Smellie J, Gimeno M J, Gómez J B, Auqué L F, Sandström B, Pedersen K, 2011. Site investigation SFR. Bedrock hydrogeochemistry. SKB R-11-06, Svensk Kärnbränslehantering AB.

Sandström B, Tullborg E-L, 2011. Site investigation SFR. Fracture mineralogy and geochemistry of borehole sections sampled for groundwater chemistry and Eh. Results from boreholes KFR01, KFR08, KFR10, KFR19, KFR7A and KFR105. SKB P-11-01, Svensk Kärnbränslehantering AB.

Sandström B, Tullborg E-L, Smellie J, MacKenzie A B, Suksi J, 2008. Fracture mineralogy of the Forsmark site. SDM-Site Forsmark. SKB R-08-102, Svensk Kärnbränslehantering AB.

Sandström B, Tullborg E-L, Larson S Å, Page L, 2009. Brittle tectonothermal evolution in the Forsmark area, central Fennoscandian Shield, recorded by paragenesis, orientation and $^{40}Ar/^{39}Ar$ geochronology of fracture minerals. Tectonophysics 478, 158–174.

Sandström B, Nilsson K, Tullborg E-L, 2011. Site investigation SFR. Fracture mineralogy including identification of uranium phases and hydrochemical characterisation of groundwater in borehole KFR106. SKB P-11-41, Svensk Kärnbränslehantering AB.

Sidborn M, Sandström B, Tullborg E-L, Salas J, Maia F, Delos A, Molinero J, Hallbeck L, Pedersen K, 2010. SR-Site: Oxygen ingress in the rock at Forsmark during a glacial cycle. SKB TR-10-57, Svensk Kärnbränslehantering AB.

Tullborg E-L, Drake H, Sandström B, 2008. Palaeohydrogeology: a methodology based on fracture mineral studies. Applied Geochemistry 23, 1881–1897.

SKB, 2008. Site description of Forsmark at completion of the site investigation phase. SDM-Site Forsmark. SKB TR-08-05, Svensk Kärnbränslehantering AB.

Öhman J, Bockgård N, Follin S, 2012. Bedrock hydrogeology. Site investigation SFR. SKB R-11-03, Svensk Kärnbränslehantering AB.

Appendix 1

Sample descriptions

Borehole: KFR102B

Adjusted borehole length: 17.45–17.49 m.

The fracture surface is dominated by two varieties of mixed layer clay. The rust-brown parts of the surface are richer in the Fe-rich variant. Small amounts of a Ca-Al-silicate, probably prehnite and amorphous (Ca,REE)PO_4 (monazite?) were also identified. No iron hydroxide was found in the fracture.

Figure A1-1. *Photo of the sampled fracture from KFR102B 17.45–17.49 m.*

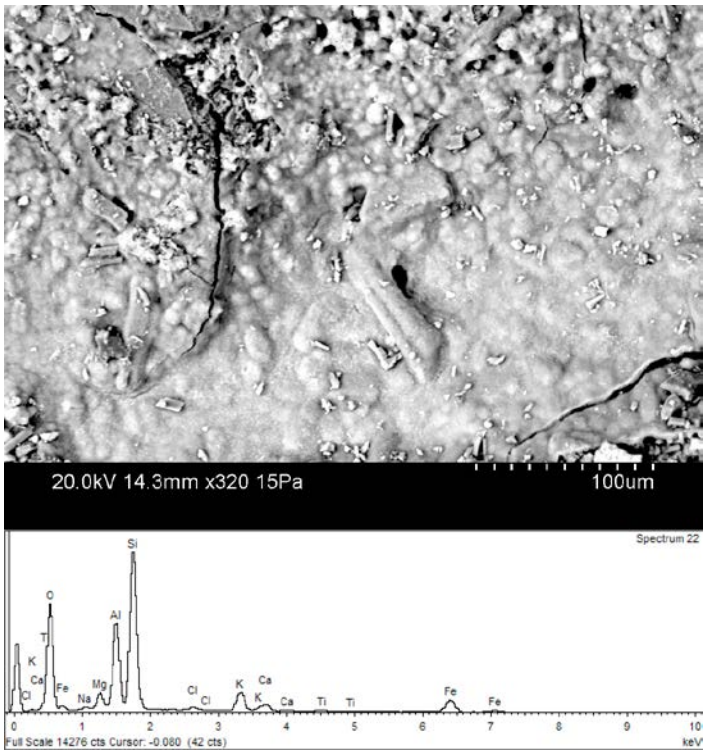

Figure A1-2. *BSE-image and EDS-spectra of clay-mineral from KFR102B 17.45–17.49 m.*

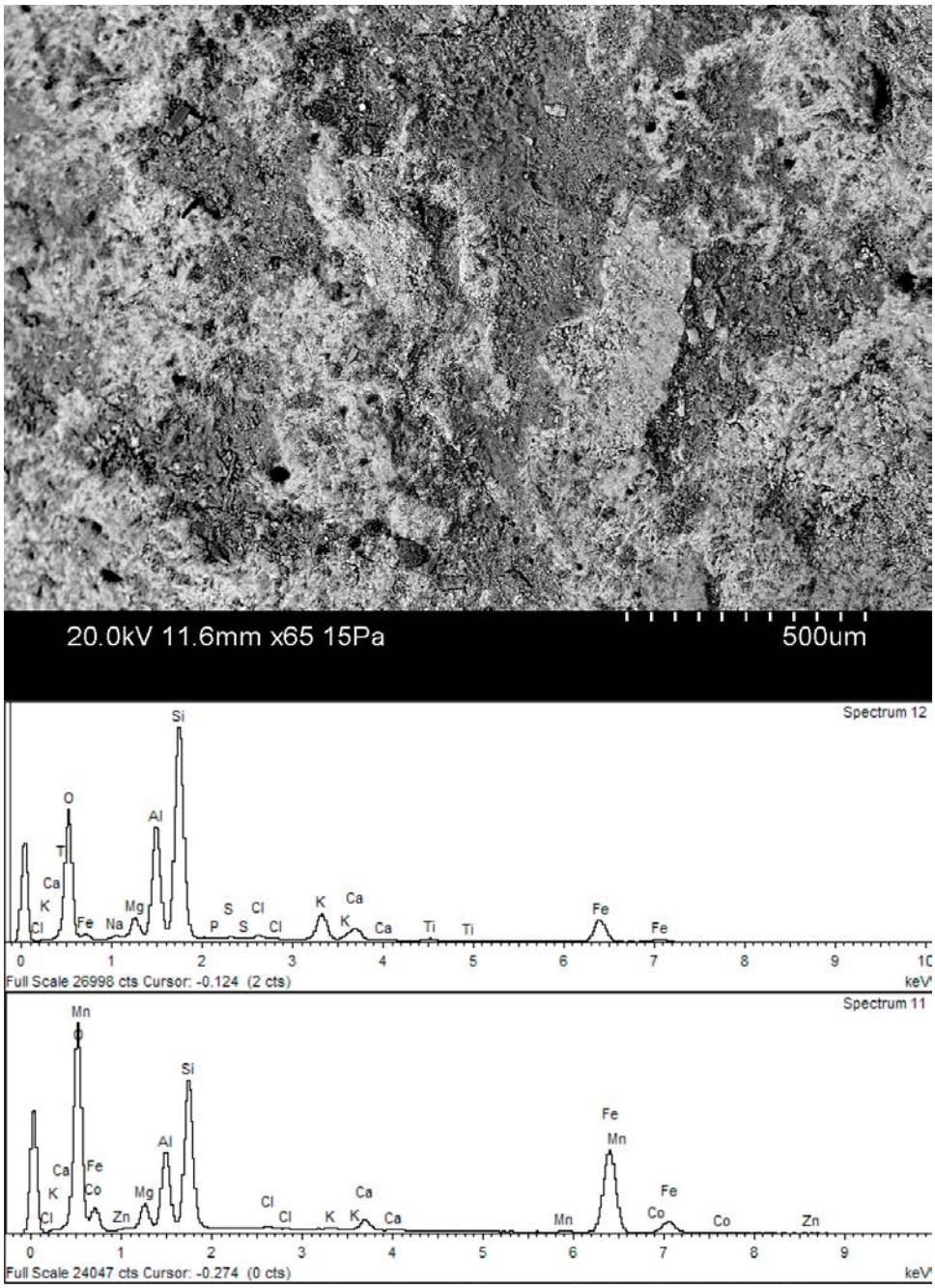

Figure A1-3. *BSE-image and EDS-spectra of two clay minerals from KFR102B 17.45–17.49 m, the bright mineral in the BSE-image and the lower spectrum is the Fe-rich clay mineral.*

Borehole: KFR102B

Adjusted borehole length: 26.76–26.91 m.

The fracture surface is coated with mixed layer clay, adularia and calcite. The rust-brown mineral consists of mixed layer clay. No iron hydroxide was found in the fracture.

Figure A1-4. *Photo of the sampled fractures from KFR102B 26.67–26.91 m.*

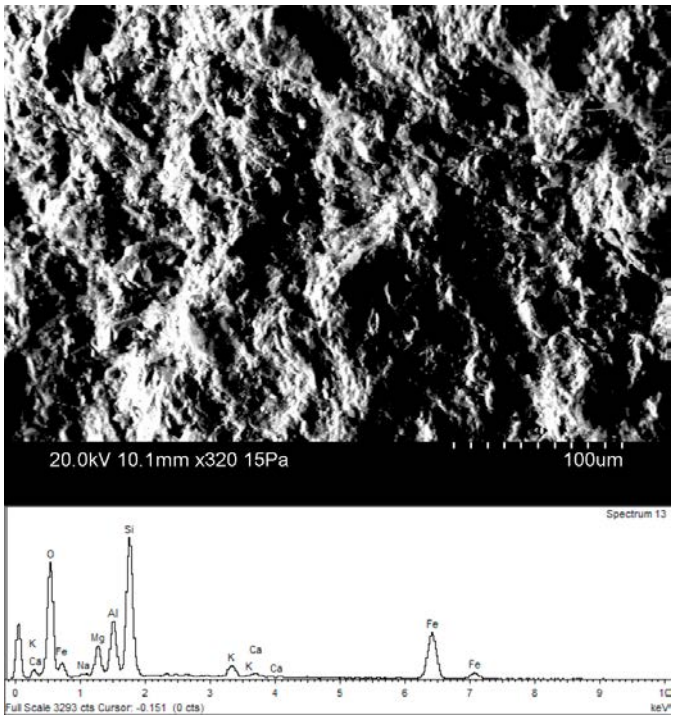

Figure A1-5. *SEM image and EDS-spectra of mixed layer clay from KFR102B 26.67–26.91 m.*

Borehole: KFR102B

Adjusted borehole length: 113.56–113.88 m.

The rust-brown colour on parts of the fracture surface consists of non-consolidated small grains (< 50 µm) of mainly clay mineral, quartz and albite. Most of the grains are subhedral. Small angular Fe-rich grains are also present within the non-consolidated material. The EDS-spectrums show very high Fe/O ratios and the presence of small amounts of Si, Al, Ca, Mg, Na. However, the spot size of the EDS (ca 10 µm) is approximately of the same size as the grains. The O, Si, Ca, Mg and Na peaks are probably due to interference from the clay minerals around the grains and on the grain surfaces. Thus, it is inferred that the Fe-rich grains consists of metallic iron or steel fragments. The rust-brown colour may be due to partial oxidation of the metallic iron/steel fragments which originates from the drilling process. No iron hydroxide was found in the fracture.

Figure A1-6. *Photo of the sampled fractures from KFR102B 113.56–113.88 m.*

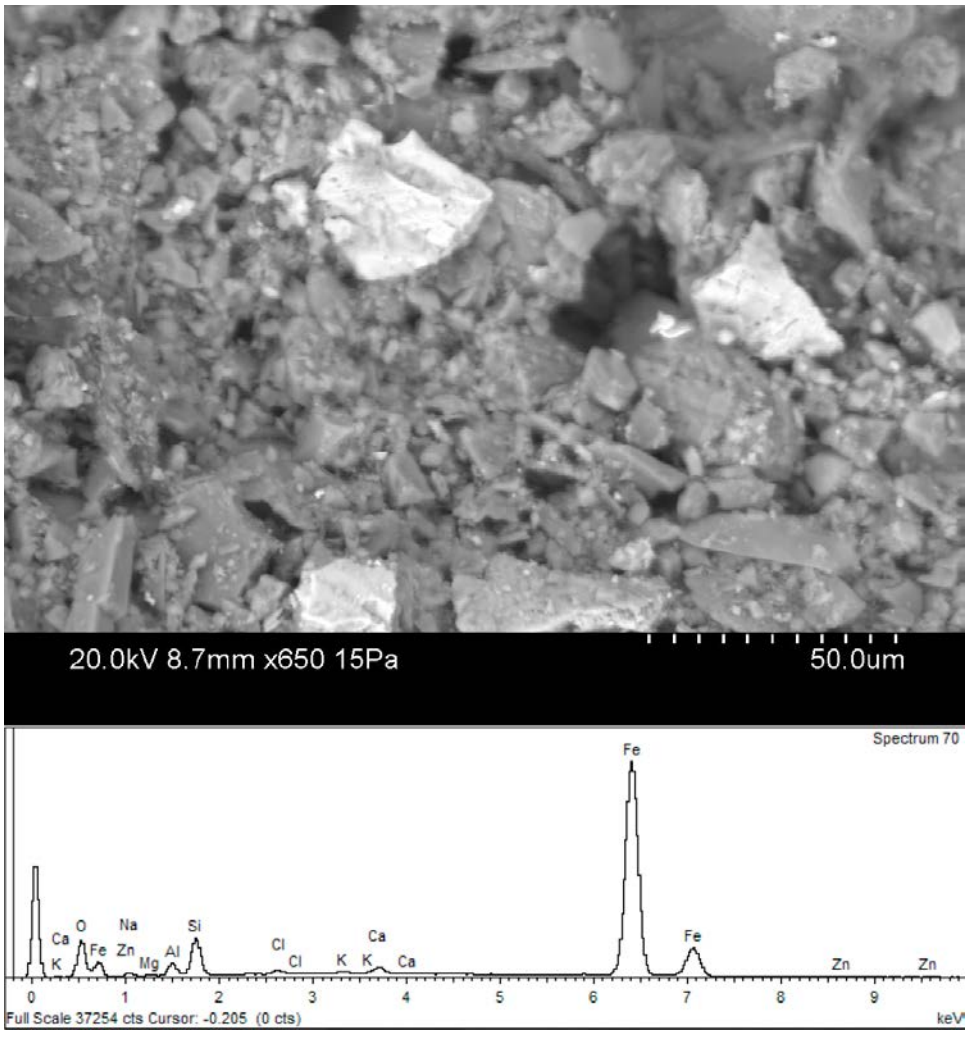

Figure A1-7. *BSE-image and EDS-spectrum of angular Fe-rich grains (bright) on fracture surface from KFR102B 113.56–113.88 m dominated by clay mineral, albite and quartz.*

Borehole: KFR104

Adjusted borehole length: 21.44–21.52 m.

The fracture surface is dominated by mixed layer clay (corrensite). U-silicate also occurs on the fracture surface as a green-brown precipitate. It contains Fe, Ca and small amounts of Pb. No iron hydroxide was found in the fracture.

Figure A1-8. *Photo of the sampled fracture from KFR104 21.44–21.52 m.*

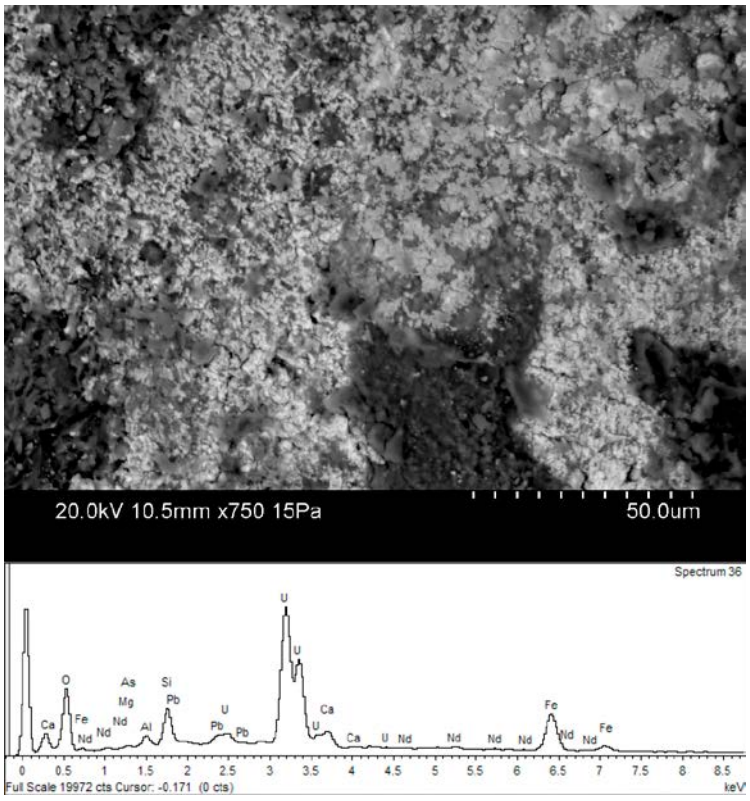

Figure A1-9. *BSE-image and EDS-spectra of U-silicate (bright) on fracture surface from KFR104 21.44–21.52 m coated with clay mineral (dark).The brighter parts of the U-mineral in the BSE-image are more Pb-rich.*

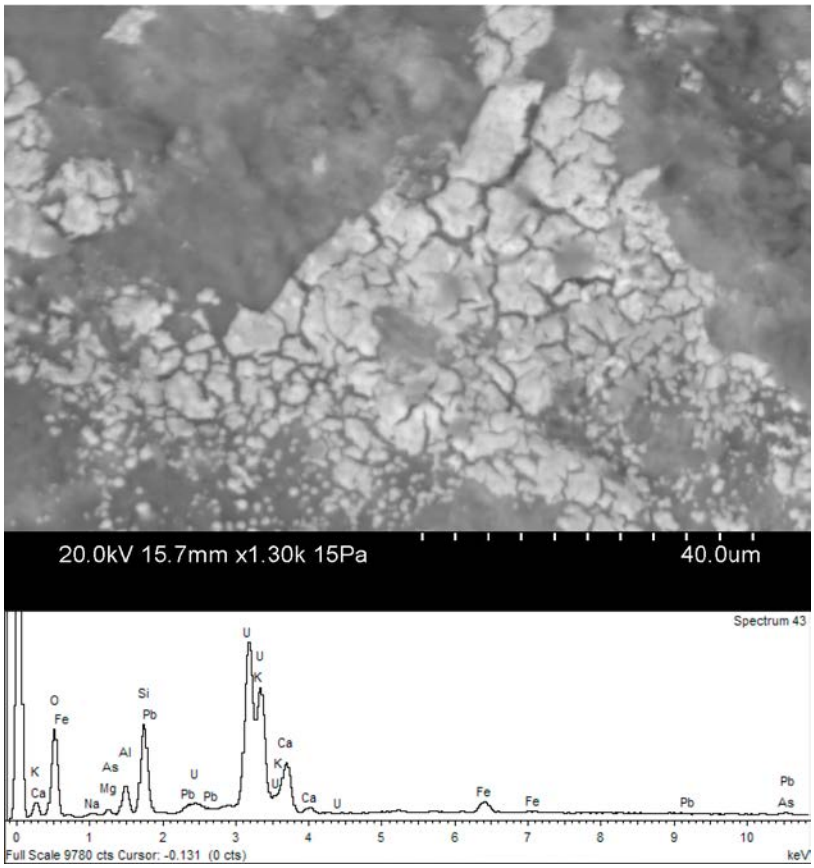

Figure A1-10. *BSE-image and EDS-spectra of U-silicate (bright) on fracture surface from KFR104 21.44–21.52 m coated with clay mineral (dark).*

Borehole: KFR104

Adjusted borehole length: 21.57–21.66 m.

The fracture surface is dominated by mixed layer clay (corrensite). The green-yellow coating seen on the surface consists of U-silicate. The U-silicate is cogenetic with barite and contains Ca, Pb and Fe. No iron hydroxide was found in the fracture.

Figure A1-11. *Photo of the sampled fracture from KFR104 21.57–21.66 m.*

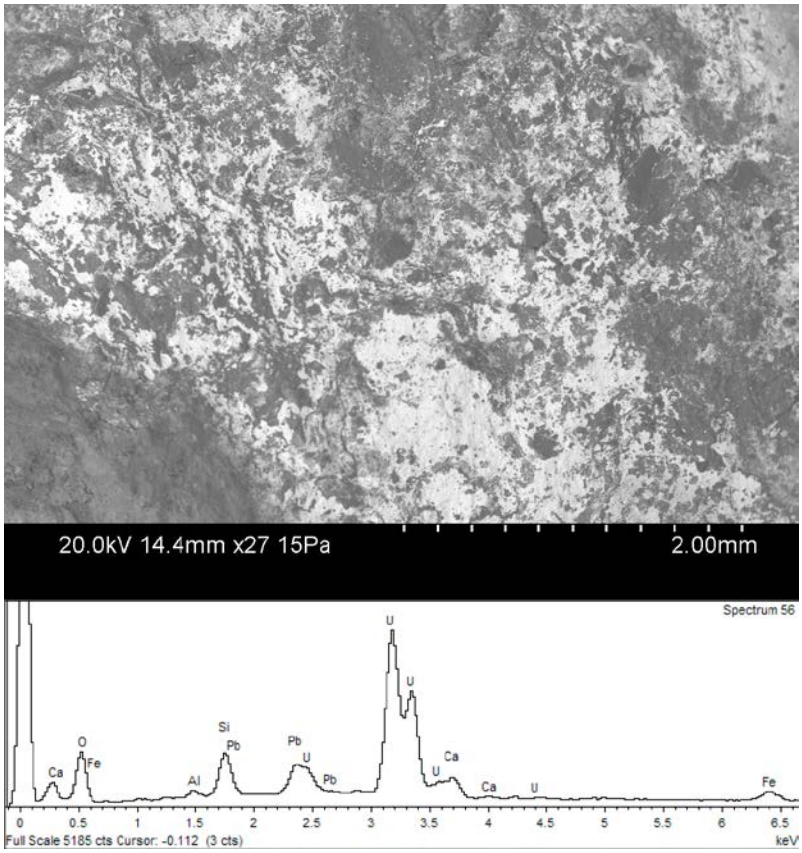

Figure A1-12. *BSE-image and EDS-spectra of U-silicate (bright) on fracture surface from KFR104 21.57–21.66 m coated with clay mineral (dark).*

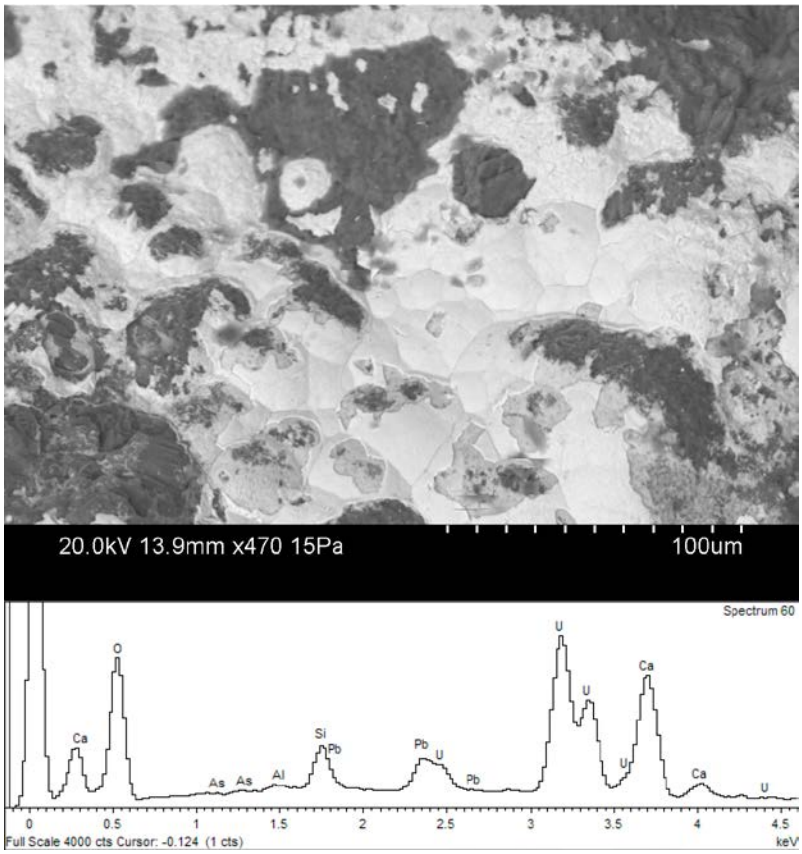

Figure A1-13. *BSE-image and EDS-spectra of a (Ca)U-silicate (bright) on fracture surface from KFR104 21.57–21.66 m coated with clay mineral (dark).*

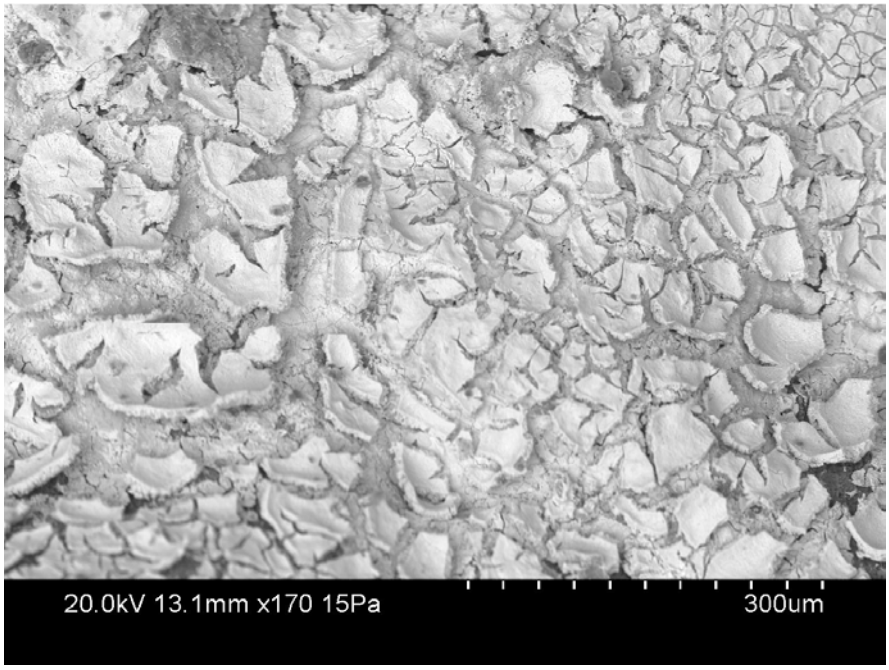

Figure A1-14. *BSE-image of U-oxide (bright) on fracture surface from KFR104 21.57–21.66 m coated with clay mineral (dark).*

Borehole: KFR104

Adjusted borehole length: 24.80–24.88 m.

The fracture surface is coated with mixed layer clay, calcite, illite, hematite, U-phosphate. No iron hydroxide was found in the fracture.

Figure A1-15. *Photo of the sampled fracture from KFR104 24.80–24.88 m.*

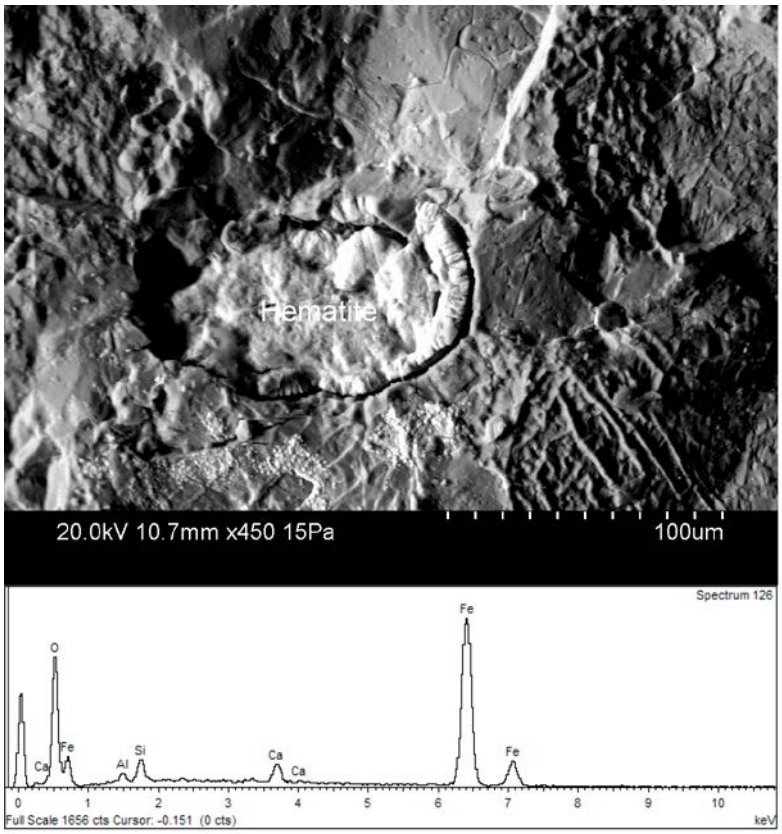

Figure A1-16. *BSE-image and EDS-spectra of hematite grain on fracture surface from KFR104 24.80–24.88 m.*

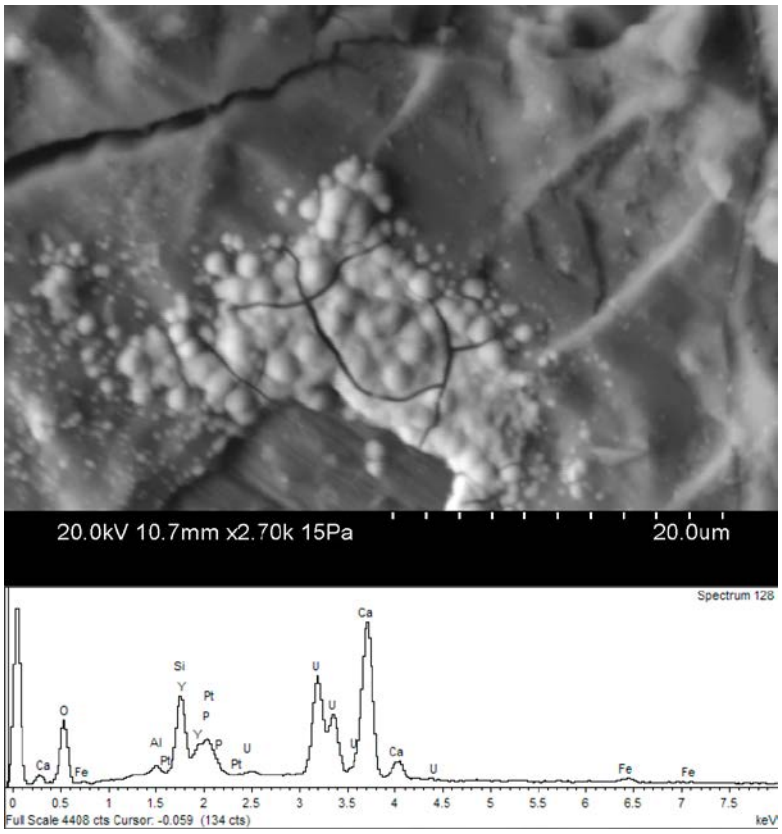

Figure A1-17. *BSE-image and EDS-spectra of U-phosphate on fracture coating calcite from KFR104 24.80–24.88 m. The Ca peak is from calcite beneath the U-phosphate.*

Borehole: KFR104

Adjusted borehole length: 25.03–25.09 m.

The fracture surface is dominated my mixed layer clay and adularia. A few small occurrences of U-silicate were also identified. The rust-brown parts of the fracture consist of Fe-rich mixed layer clay. No iron hydroxide was detected on the fracture surface.

Figure A1-18. *Photo of the sampled fracture from KFR104 25.03–25.09 m.*

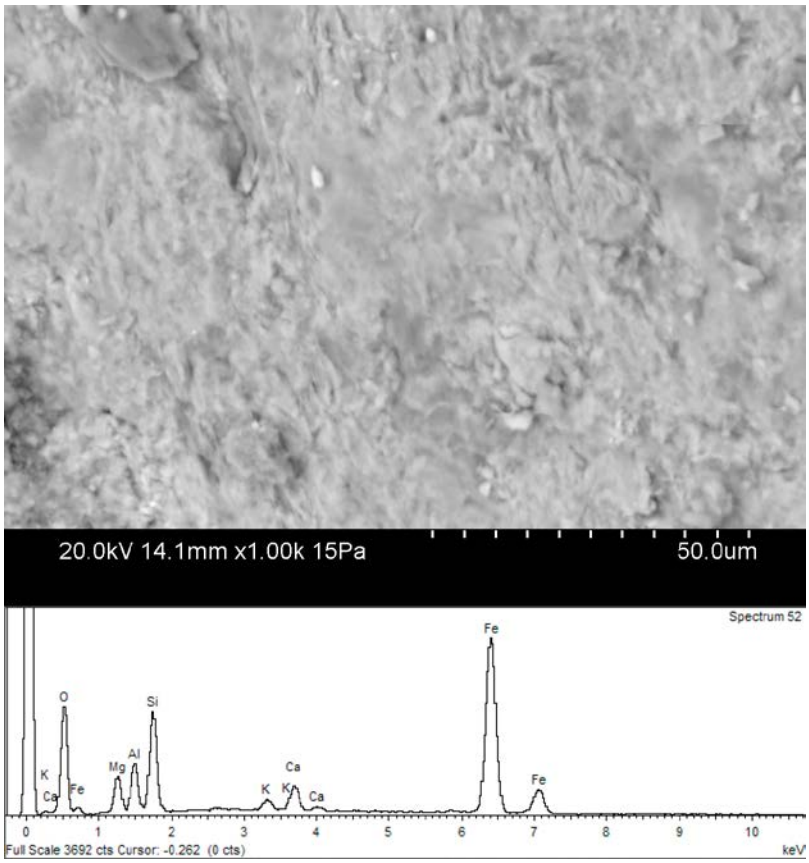

Figure A1-19. *BSE-image and EDS-spectra of Fe-rich mixed layer clay on fracture surface KFR104 25.03–25.09 m.*

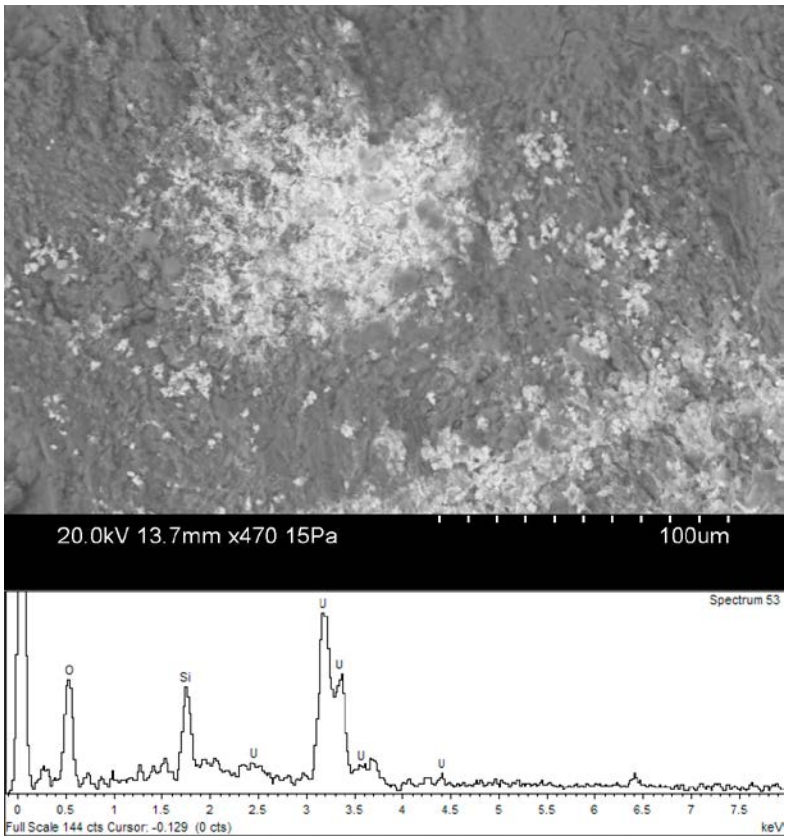

Figure A1-20. *BSE-image and EDS-spectra of U-silicate on fracture surface from KFR104 25.03–25.09 m coated with clay mineral.*

Borehole: KFR104

Adjusted borehole length: 25.51–25.62 m.

The fracture is coated with mixed layer clay and barite. U-silicate occurs closely related to the barite. A few minute-grains of galena and monazite are also present on the surface. In the rust-brown parts of the sample, the clay mineral is very Fe-rich (up to approximately 50–60wt% Fe_2O_3 total) and is the cause of the rust-brown colour on the fracture surface. No iron hydroxide was found in the fracture.

Figure A1-21. *Photo of the sampled fracture from 25.51–25.62 m.*

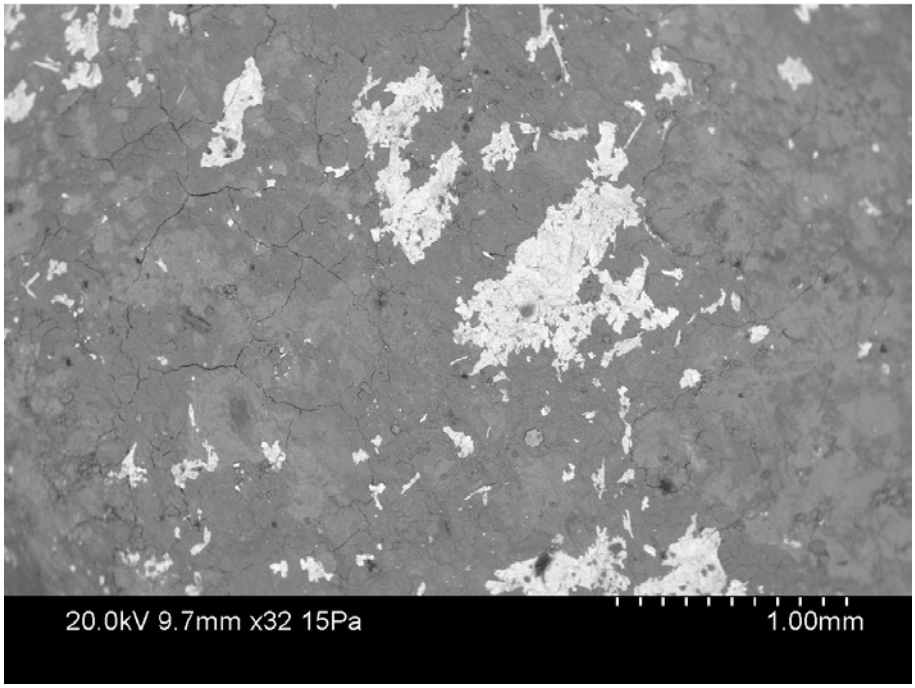

Figure A1-22. *BSE-image of barite (bright) on fracture surface from 25.51–25.62 m coated with mixed layer clay.*

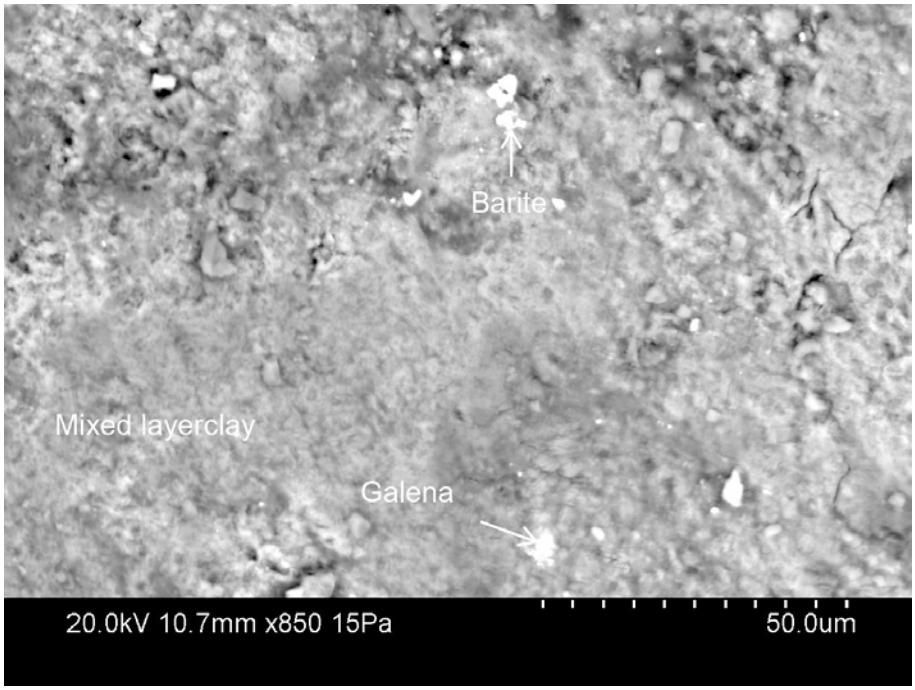

Figure A1-23. *BSE-image of small precipitates of galena and barite on fracture surface from 25.51–25.62 mcoated with mixed layer clay.*

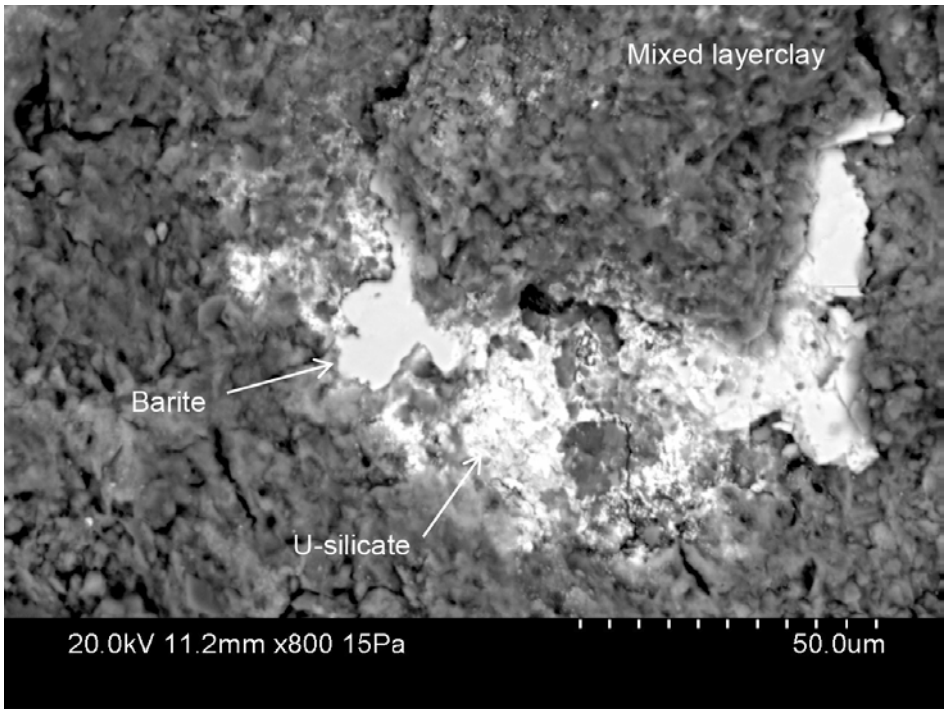

Figure A1-24. *BSE-image of U-silicate together with barite on fracture surface from 25.51–25.62 m coated with mixed layer clay.*

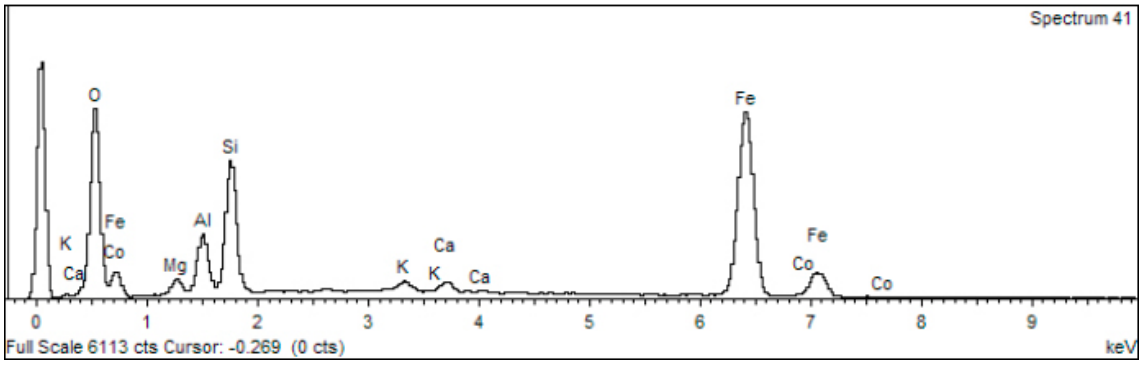

Figure A1-25. *EDS-spectra of Fe-rich mixed layer clay from 25.51–25.62 m.*

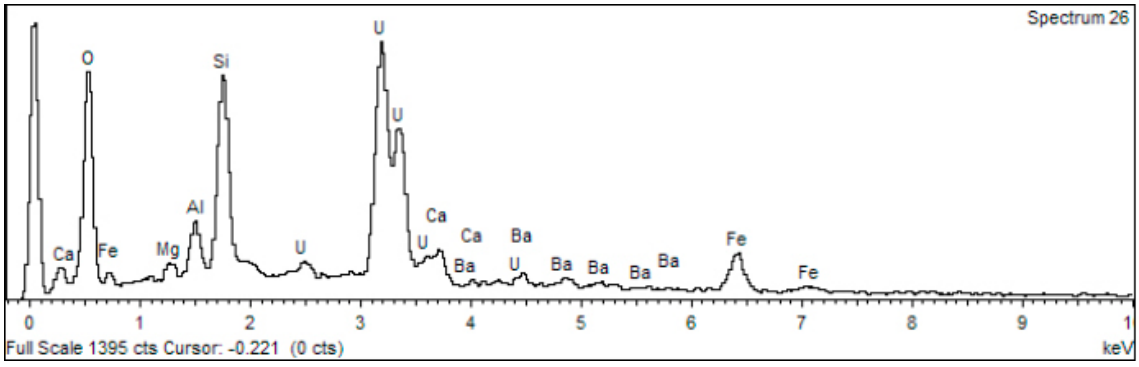

Figure A1-26. *EDS-spectra of U-silicate from 25.51–25.62 m.*

Borehole: KFR104

Adjusted borehole length: 27.04–27.11 m.

The fracture surface is coated with mixed layer clay and illite, the rust-brown parts of the fracture consists of Fe-rich mixed layer clay. No iron hydroxide was found in the fracture.

Figure A1-27. *Photo of the sampled fracture from 27.04–27.11 m.*

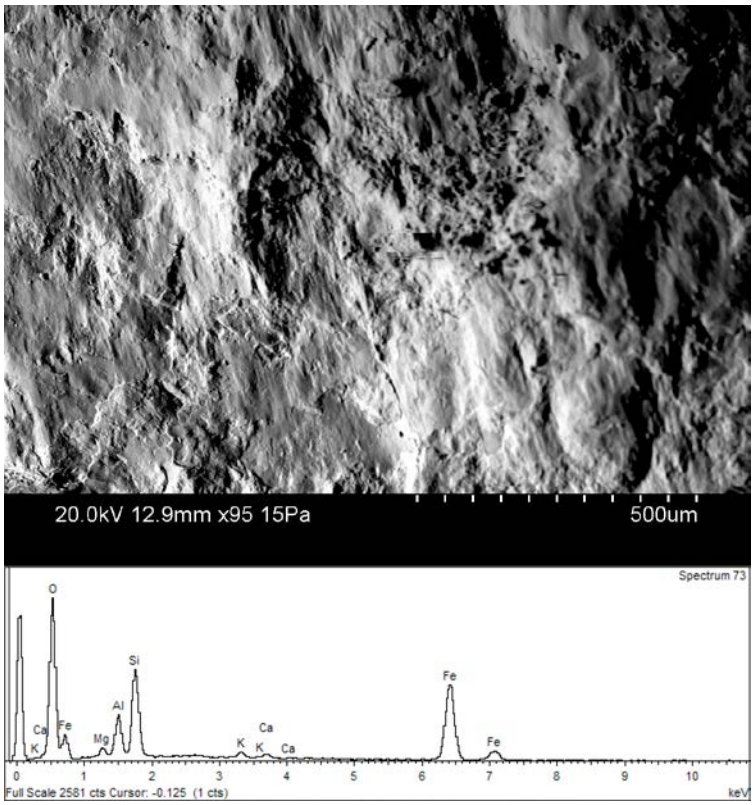

Figure A1-28. *SEM image and EDS-spectra of U-silicate on fracture surface from KFR104 27.04–27.11 m coated with clay mineral.*

Borehole: KFR104

Adjusted borehole length: 29.80–29.93 m.

The fracture surface is dominated by mixed layer clay and adularia. A few small occurrences of barite and U-phosphate were also found on the surface. No iron hydroxide was found in the fracture

Figure A1-29. *Photo of the sampled fracture from KFR104 29.80–29.93 m.*

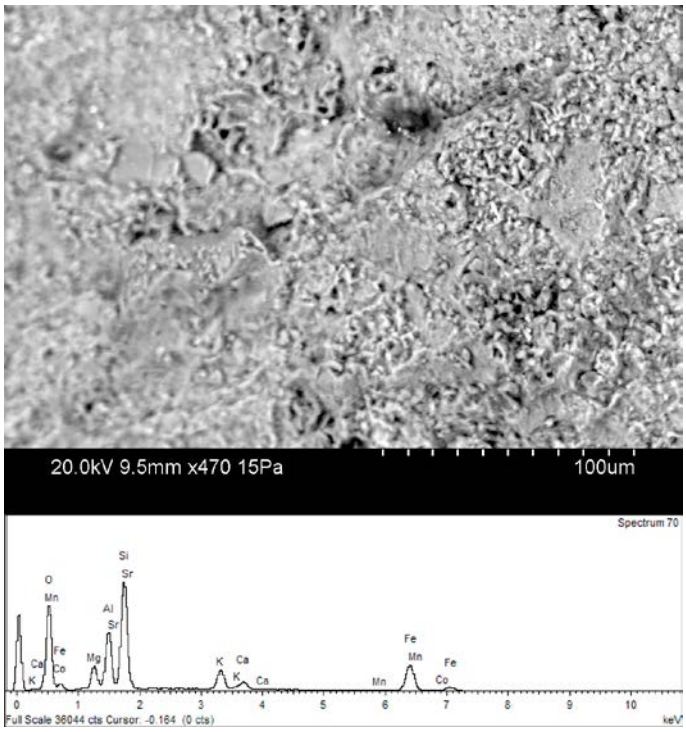

Figure A1-30. *BSE-image and EDS-spectra of clay mineral coating on fracture surface from KFR104 29.80–29.93 m.*

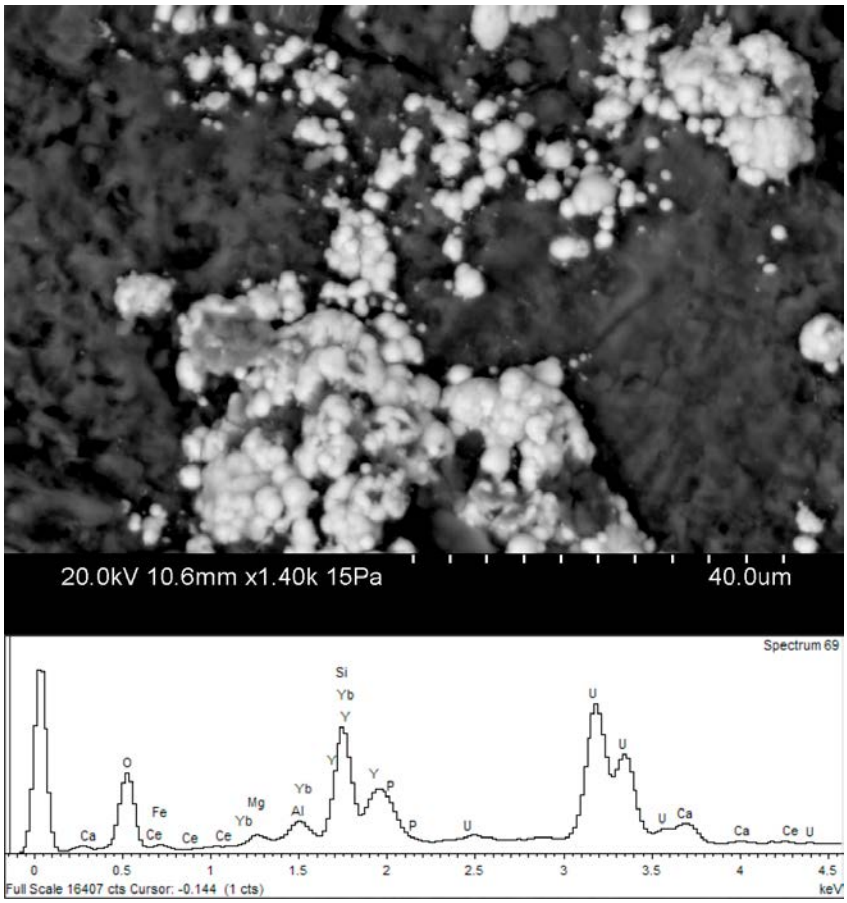

Figure A1-31. *BSE-image and EDS-spectra of U-phosphate on fracture from KFR104 29.80–29.93 m coated with clay mineral.*

Borehole: KFR104

Adjusted borehole length: 30.20–30.28 m.

The fracture coating is dominated by laumontite, chlorite and mixed layer clay. The rust-brown mineral is hematite. No iron hydroxide was found in the fracture.

Figure A1-32. *Photo of the sampled fracture from KFR104 30.20–30.28 m.*

Borehole: KFR104

Adjusted borehole length: 32.67–32.76 m.

The fracture coating is dominated by mixed layer clay. Small amounts of U-phosphate are also present on the fracture (green-brown). No iron hydroxide was found in the fracture.

Figure A1-33. *Photo of the sampled fracture from KFR104 32.67–32.76 m.*

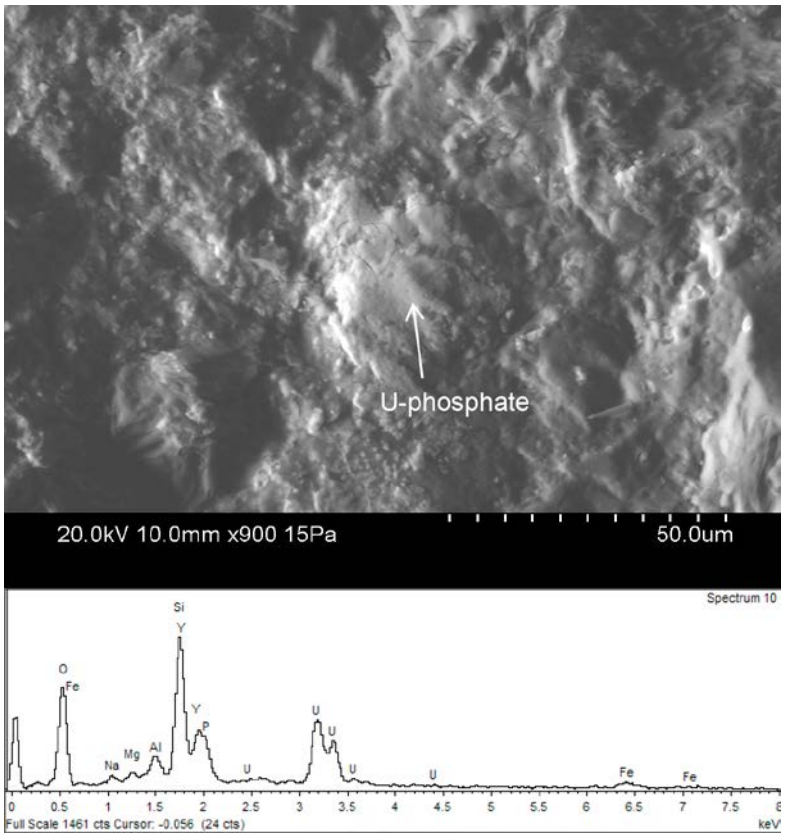

Figure A1-34. *SEM image and EDS-spectra of U-phosphate on fracture surface from KFR104 32.67–32.76 m.*

Borehole: KFR104

Adjusted borehole length: 43.53–43.76 m.

The red-coloured mineral is hematite-stained albite and adularia. These minerals are part of older sealed fractures which have been reactivated and coated with mixed layer clay. Small grains of (Ca,REE)-carbonate are also found on the fracture surface. No iron hydroxide was found in the fracture.

Figure A1-35. *Photo of the sampled fractures from KFR104 43.53–43.76 m.*

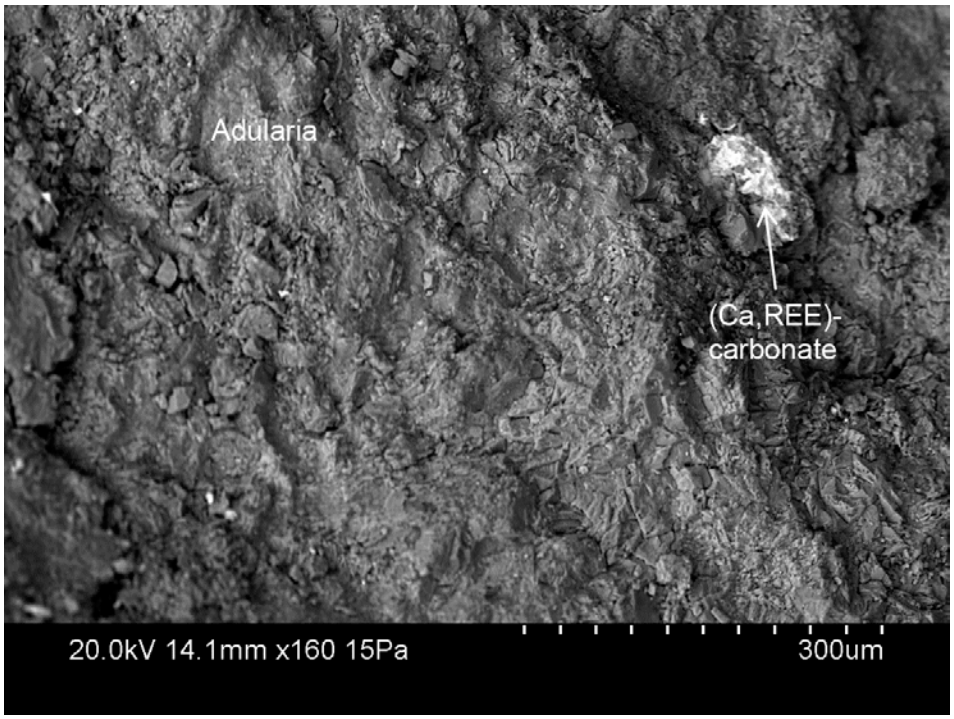

Figure A1-36. *BSE-image of (Ca,REE)-carbonate on adularia from KFR104 43.53–43.76 m.*

Borehole: KFR104

Adjusted borehole length:55.95–56.04 m.

The fracture surface is coated with mixed layer clay and illite, the rust-brown parts of the fracture surface consists of Fe-rich mixed layer clay. No iron hydroxide was found in the fracture.

Figure A1-37. *Photo of the sampled fractures from KFR104 55.95–56.04 m.*

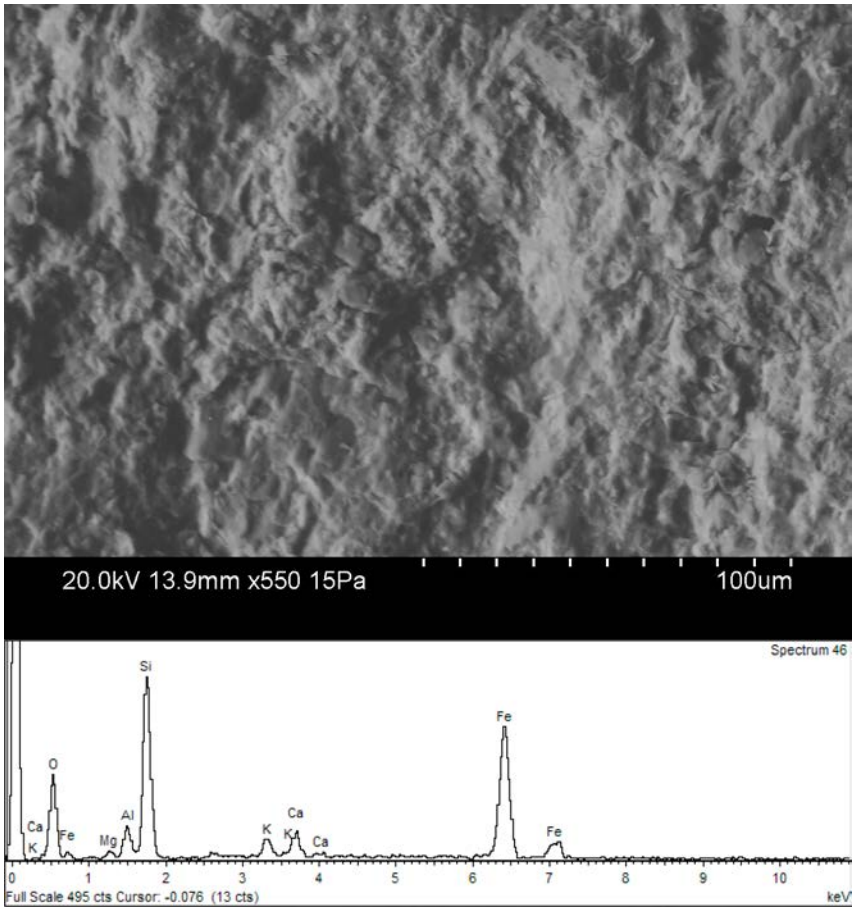

Figure A1-38. *SEM image and EDS-spectra of Fe-rich mixed layer clay from KFR104 55.95–56.04 m.*

Borehole: KFR104

Adjusted borehole length: 59.21–59.25 m.

The sample consists of a fracture in pegmatite coated with mainly hematite. The rust-coloured parts on the fracture surface consist of Fe-oxide with an "etched" texture, possibly iron hydroxide. Small amounts of a Fe-U-silicate also occur on the fracture surface.

Figure A1-39. *Photo of the sampled fracture from KFR104 59.21–59.25 m.*

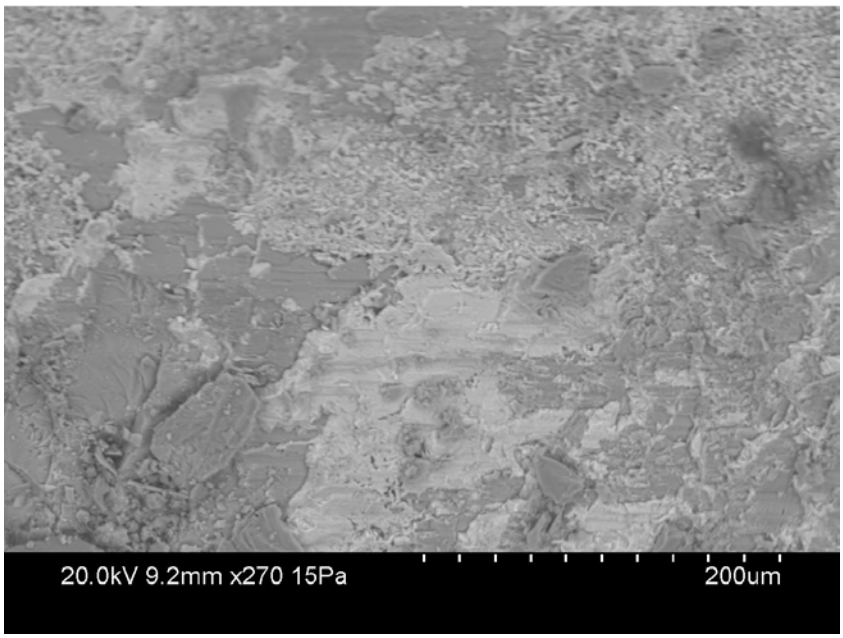

Figure A1-40. *BSE-image of hematite on fracture surface fromKFR104 59.21–59.25 m.*

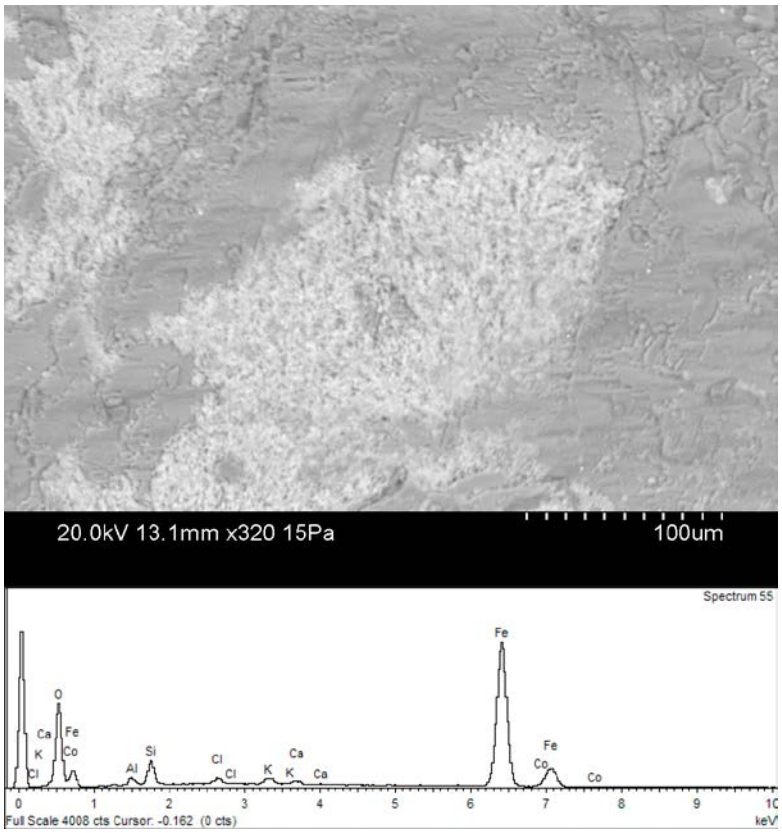

Figure A1-41. *BSE-image and EDS-spectra of Fe-oxide or possibly Fe hydroxide from KFR104 59.21–59.25 m.*

Borehole: KFR104

Adjusted borehole length: 59.71–59.75 m.

The fracture surface is coated with mainly mixed layer clay and calcite. Small grains of metallic iron (< 10 µm) are present on the fracture surface and there are drilling marks on the side of the drill core. The rust-brown parts of the fracture surface consist of Fe-rich mixed layer clay. No iron hydroxide was found in the fracture.

Figure A1-42. *Photo of the sampled fracture from KFR104 59.71–59.75 m.*

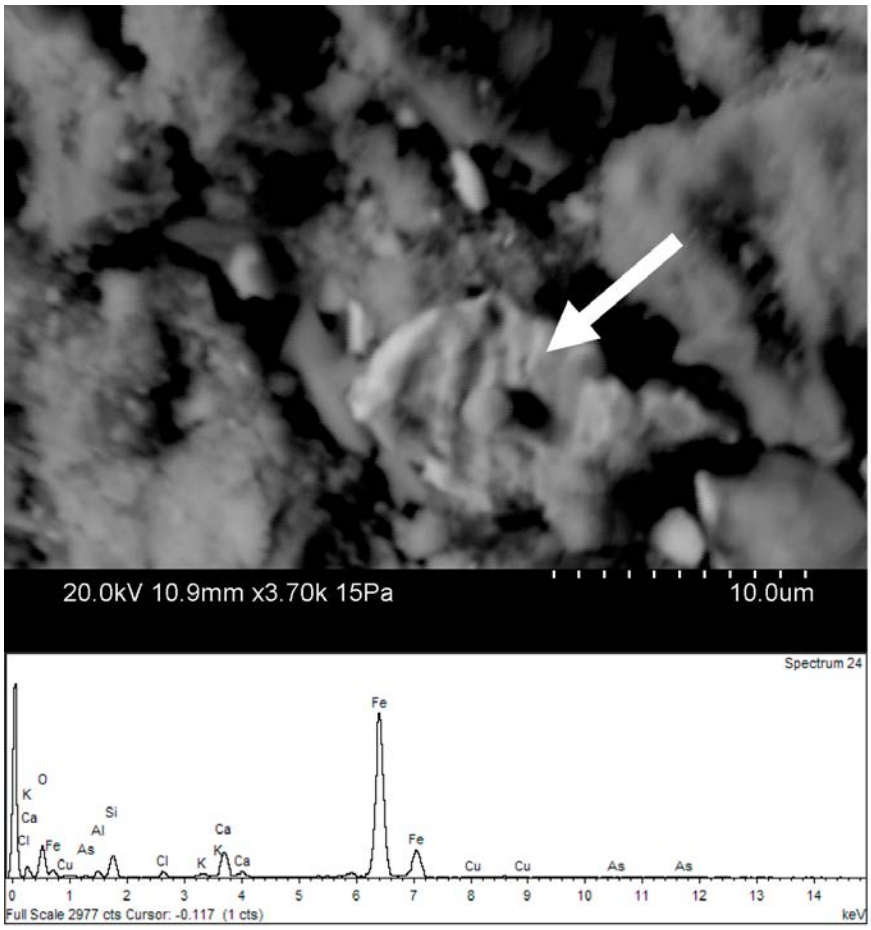

Figure A1-43. *BSE-image and EDS-spectra of metallic Fe grain from KFR104 59.71–59.75 m.*

Borehole: KFR104

Adjusted borehole length: 61.55–61.93 m.

The fractures are dominated by mixed layer clay (corrensite) and calcite. Small amounts of asphaltite, pyrite, galena, sphalerite, Zn-oxide (with small Cl-peak in EDS-spectra) are also present. Well-preserved pyrite crystals are found on the surface. No iron hydroxide was found in the fracture.

Figure A1-44. *Photo of the sampled fractures from KFR104 61.55–61.93 m.*

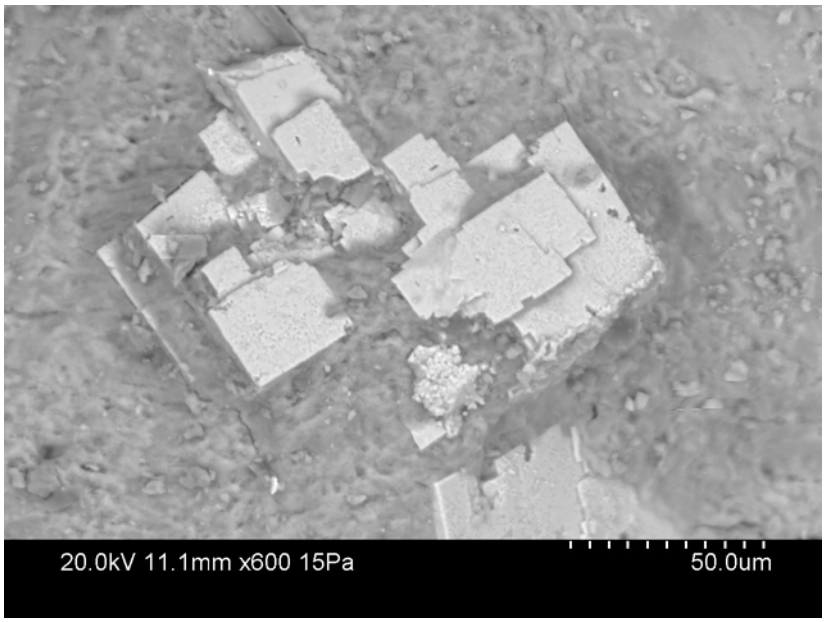

Figure A1-45. *BSE-image of well-preserved cubic pyrite crystals in mixed layer clay from KFR104 61.55–61.93 m.*

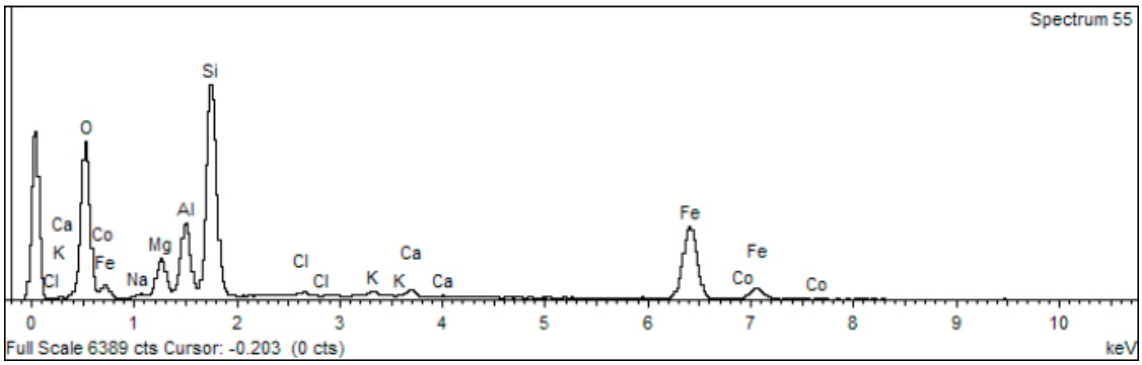

Figure A1-46. *EDS-spectra of the mixed layer clay from KFR104 61.55–61.93 m.*

Borehole: KFR104

Adjusted borehole length: 99.32–99.42 m.

The fracture surface is coated with mixed layer clay, laumontite, U-silicate, possible iron hydroxide and (Ca,REE)-carbonate.

Figure A1-47. *Photo of the sampled fractures from KFR104 99.32–99.42 m.*

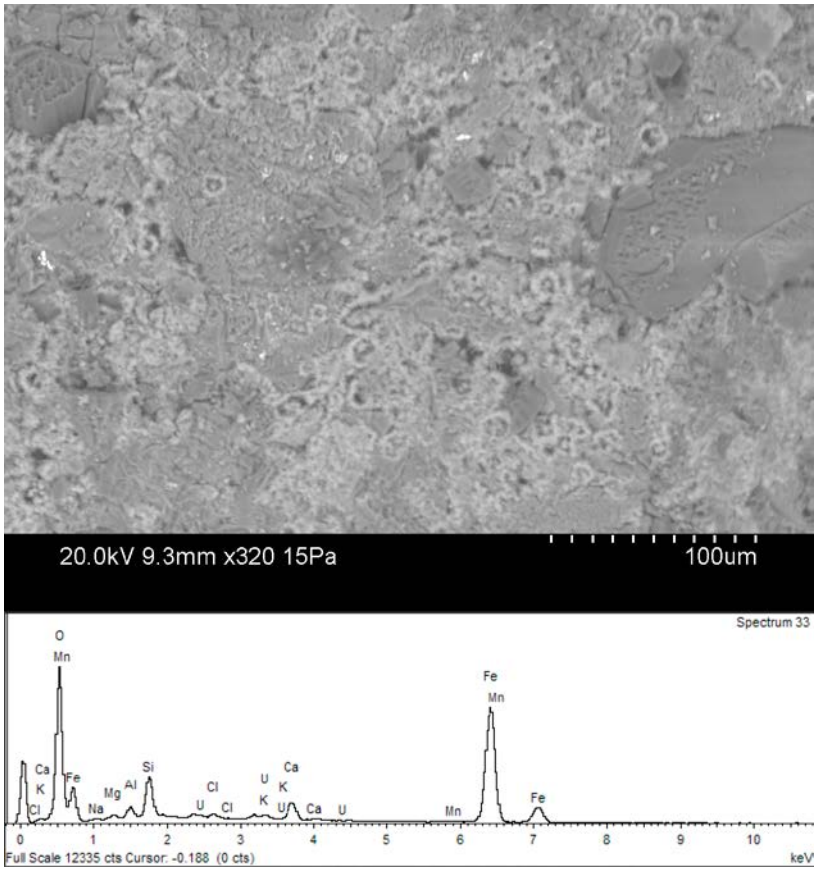

Figure A1-48. *BSE-image and EDS-spectra of Fe hydroxide from KFR104 99.32–99.42 m.*

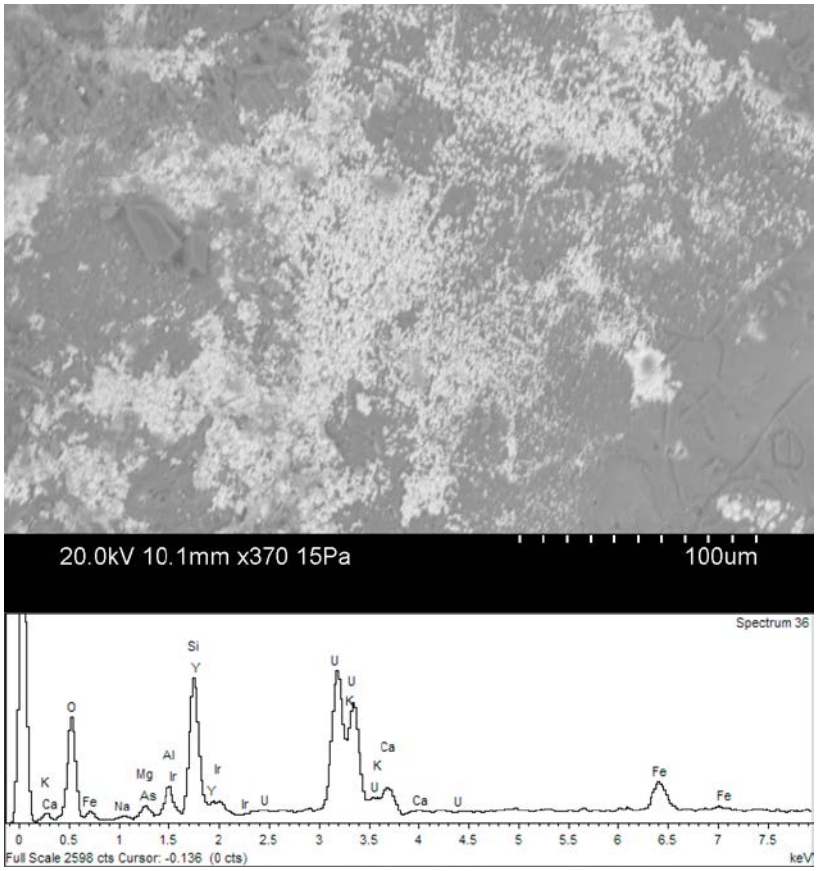

Figure A1-49. *BSE-image and EDS-spectra of U silicate from KFR104 99.32–99.42 m.*

Borehole: KFR104

Adjusted borehole length: 107.64–107.83 m.

The fracture surface is coated with laumontite and mixed layer clay.No iron hydroxide was found in the fracture.

Figure A1-50. *Photo of the sampled fracture from KFR104 107.64–107.83 m.*

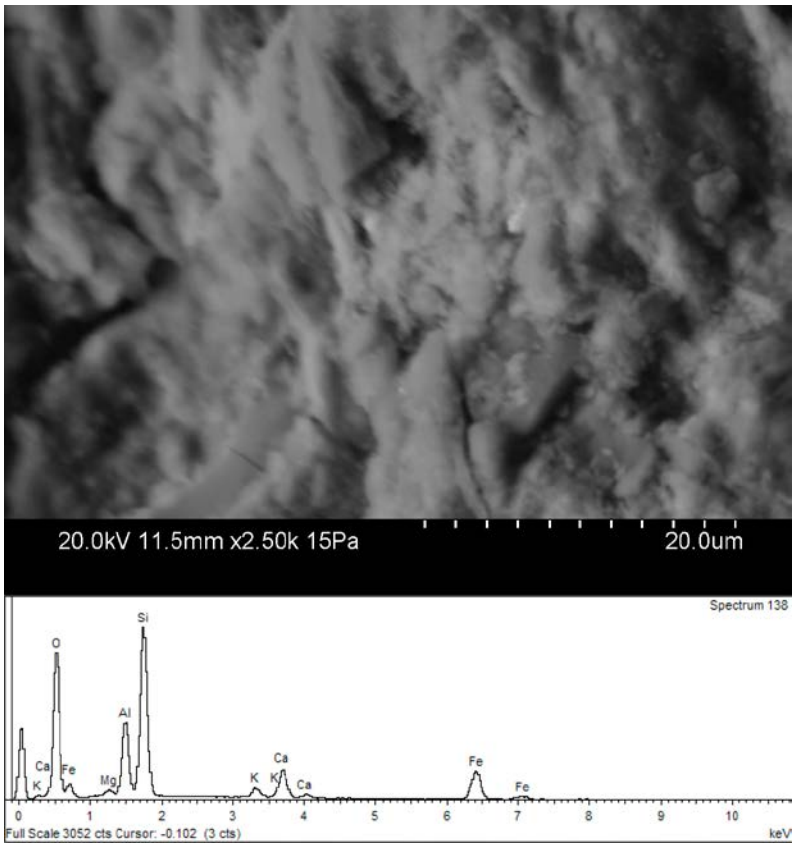

Figure A1-51. *BSE-image and EDS-spectra of mixed layer clay from KFR104 107.64–107.83 m.*

Borehole: KFR104

Adjusted borehole length: 122.52–122.56 m.

Well preserved pyrite crystals are present on the fracture surface.The rust brown parts of the fracture surface consist of debris from the drilling process. No iron hydroxide was found in the fracture.

Figure A1-52. *Photo of the sampled fracture from KFR104 122.52–122.56 m.*

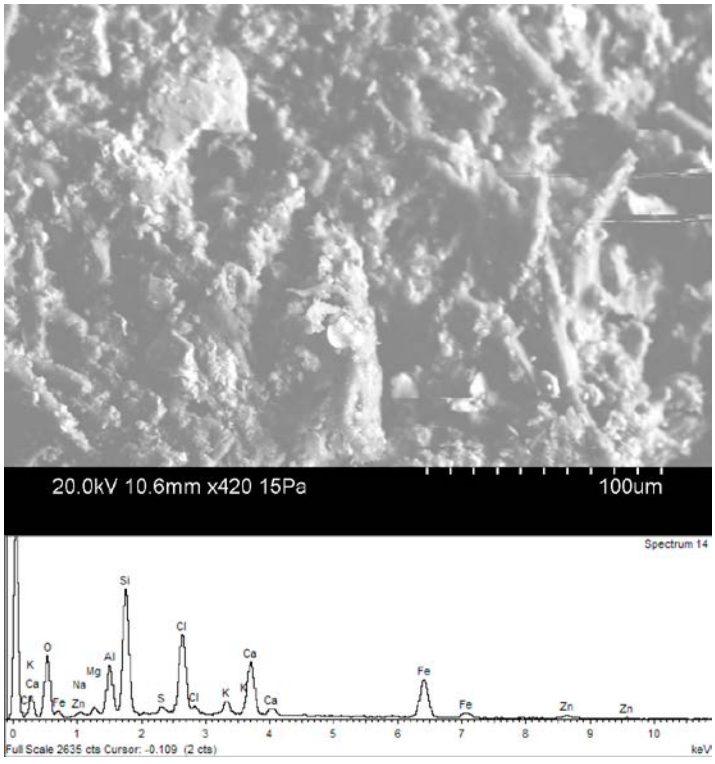

Figure A1-53. *SEM image and EDS-spectra of debris on the surface from KFR104 122.52–122.56 m.*

Borehole: KFR104

Adjusted borehole length: 134.70–134.75 m

The fracture is coated with laumontite, calcite and adularia. The rust-brown mineral consists of adularia.No iron hydroxide was found in the fracture.

Figure A1-54. *Photo of the sampled fracture from KFR104 134.70–134.75 m.*

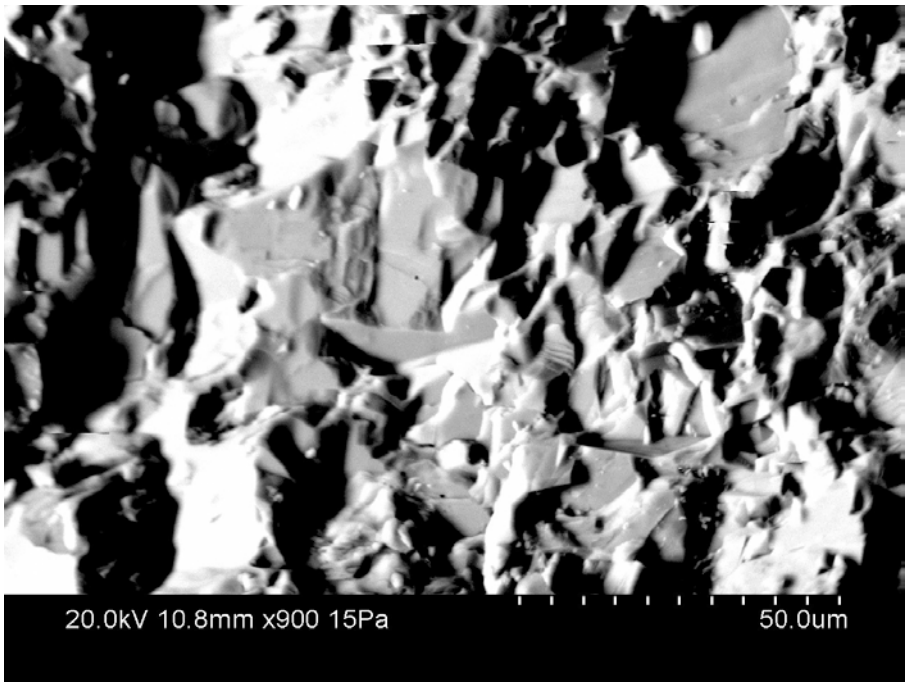

Figure A1-55. *SEM image of mixed layer clay from KFR104 134.70–134.75 m.*

Borehole: KFR104

Adjusted borehole length: 270.17–270.23 m

The fracture surface is coated with prehnite, hematite-stained adularia, and Fe-rich mixed layer clay. The rust-brown parts of the fracture consist of a mixture of prehnite and mixed layer clay. No iron hydroxide was found in the fracture.

Figure A1-56. *Photo of the sampled fracture from KFR104 270.17–270.23 m.*

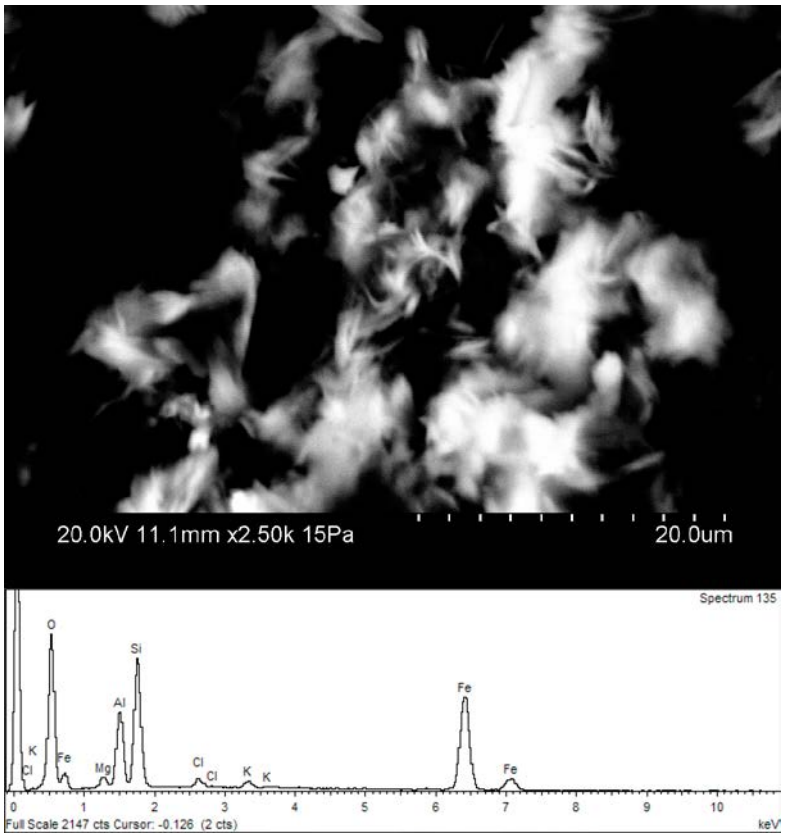

Figure A1-57. *SEM image and EDS-spectra of mixed layer clay from KFR104 270.17–270.23 m.*

Borehole: KFR104

Adjusted borehole length: 280.54–280.61 m.

The fracture surface is coated with mixed layer clay, laumontite and hematite. No iron hydroxide was found in the fracture.

Figure A1-59. *BSE-image and EDS-spectra of hematite on fracture surface from KFR104 280.54–280.61 m.*

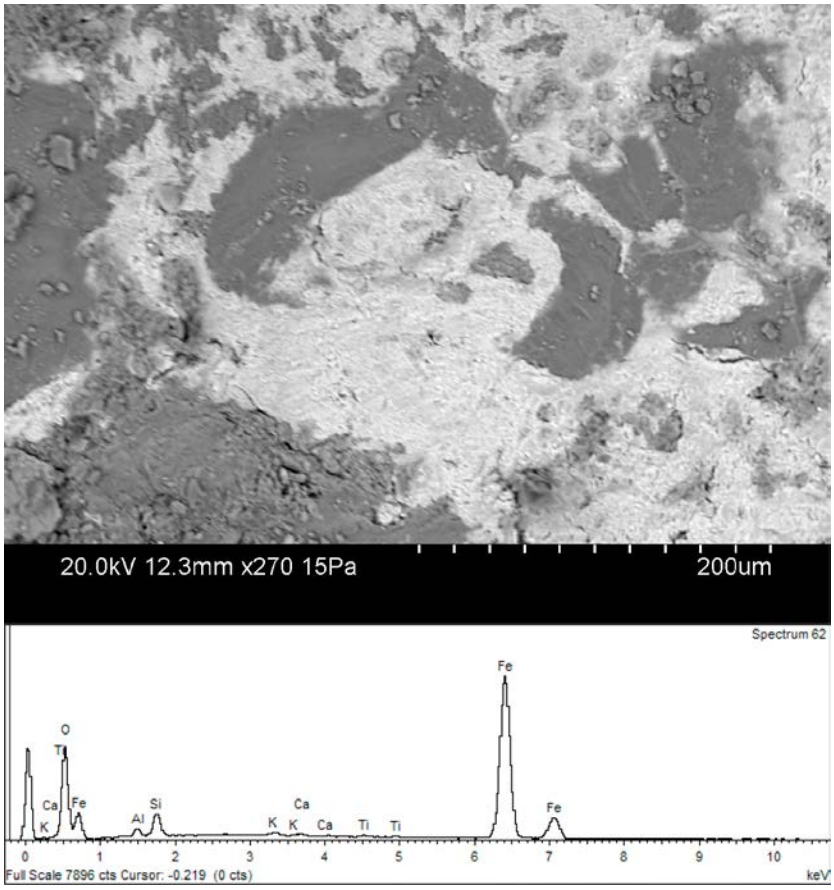

Figure A1-58. *Photo of the sampled fracture from KFR104 280.54–280.61 m.*

Borehole: KFR104

Adjusted borehole length: 293.23–293.29 m

The fracture surface is coated with mixed layer clay and illite, small grains of Fe-oxide are also present on the surface.Based on the presence of Co in the EDS-spectra, it is inferred that the Fe-oxide grains are an artefact from the drilling process.

Figure A1-60. *Photo of the sampled fracture from KFR104 293.23–293.29 m.*

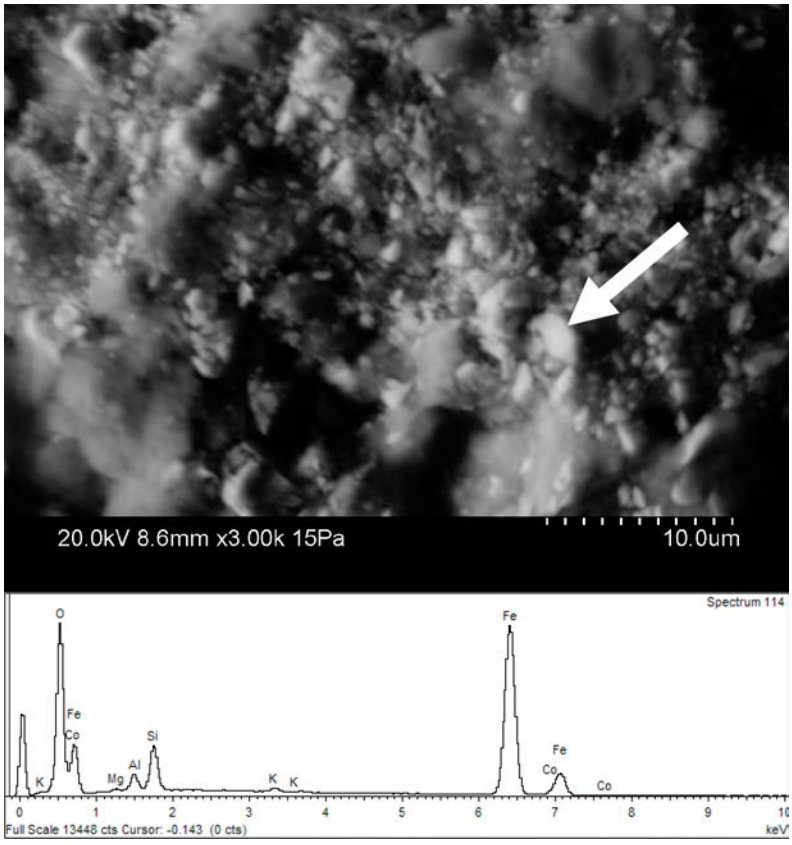

Figure A1-61. *BSE-image and EDS-spectra of Fe-grains (arrow) on mixed layer clay from KFR104 280.54–280.61 m.*

Borehole: KFR104

Adjusted borehole length: 294.02–294.15 m

The fracture surface is coated with hematite-stained adularia, albite, chlorite/corrensite, clay minerals and pyrite. No iron hydroxide was found in the fracture.

Figure A1-62. *Photo of the sampled fractures from KFR104 294.02–294.15 m.*

Borehole: KFR104

Adjusted borehole length: 328.75–328.86 m

The fracture surface is coated with mixed layer clay and small amount of U-silicate. No iron hydroxide was found in the fracture.

Figure A1-63. *Photo of the sampled fracture from KFR104 328.75–328.86 m.*

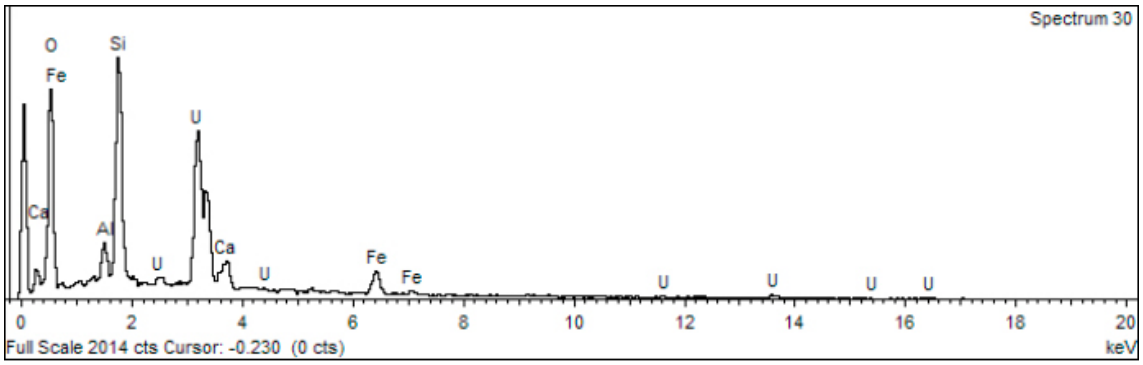

Figure A1-64. *EDS-spectra of U-silicate from KFR104 328.75–328.86 m.*

Borehole: KFR104

Adjusted borehole length: 389.97–390.03 m

Mixed layer clay, adularia,U-silicate, pyrite.Small grains of metallic iron with etched surface. The metallic iron is also present on the side of the drill core. No iron hydroxide was found in the fracture.

Figure A1-65. *Photo of the sampled fracturefrom KFR104 389.97–390.03 m.*

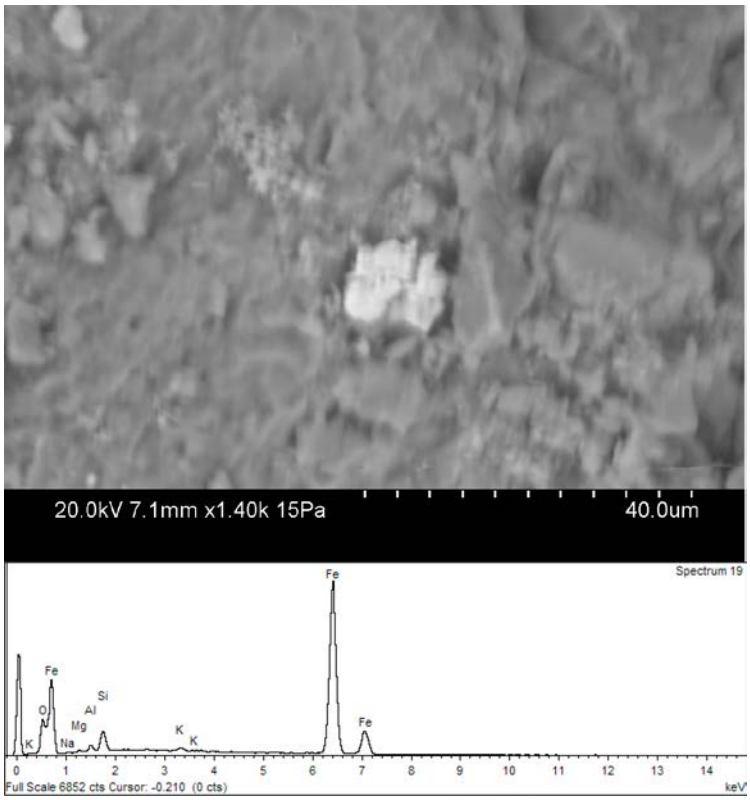

Figure A1-66. *BSE-image and EDS-spectra of small grain of metallic iron on fracture coated with mixed layer clay from KFR104 389.97–390.03 m.*

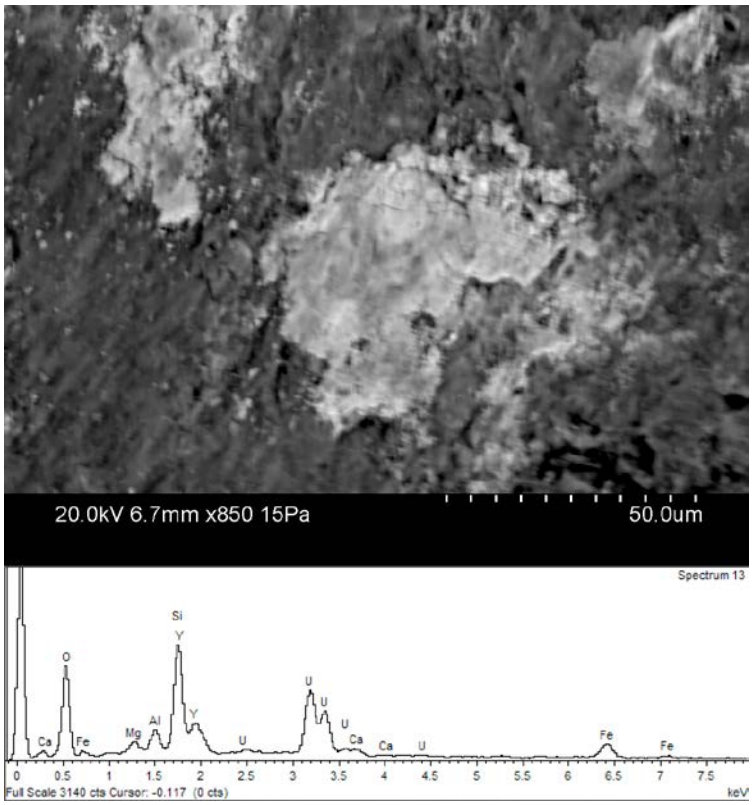

Figure A1-67. *BSE-image and EDS-spectra of U-silicate on mixed layer clay from KFR104 389.97–390.03 m.*

Borehole: KFR104

Adjusted borehole length: 416.96–417.35 m

The sample is dominated by mixed layer clays (corrensite and illite/smectite). The red-coloured parts of the clay mineral contain around 30–35 wt% Fe_2O_3total.Small grains of galena are found on the surface of the Fe-rich clay mineral. No iron hydroxide was found in the fracture.

Figure A1-68. *Photo of the sampled fractures from KFR104 416.96–417.35 m.*

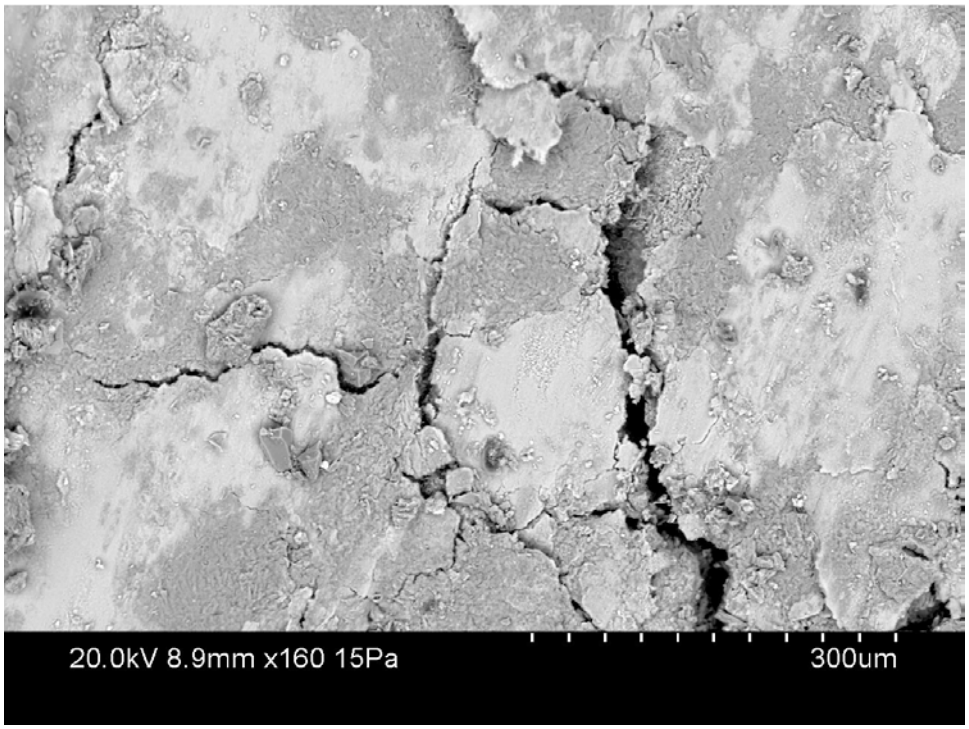

Figure A1-69. *BSE-image of mixed layer clay from KFR104 416.96–417.35 m, the brighter parts are more Fe-rich.*

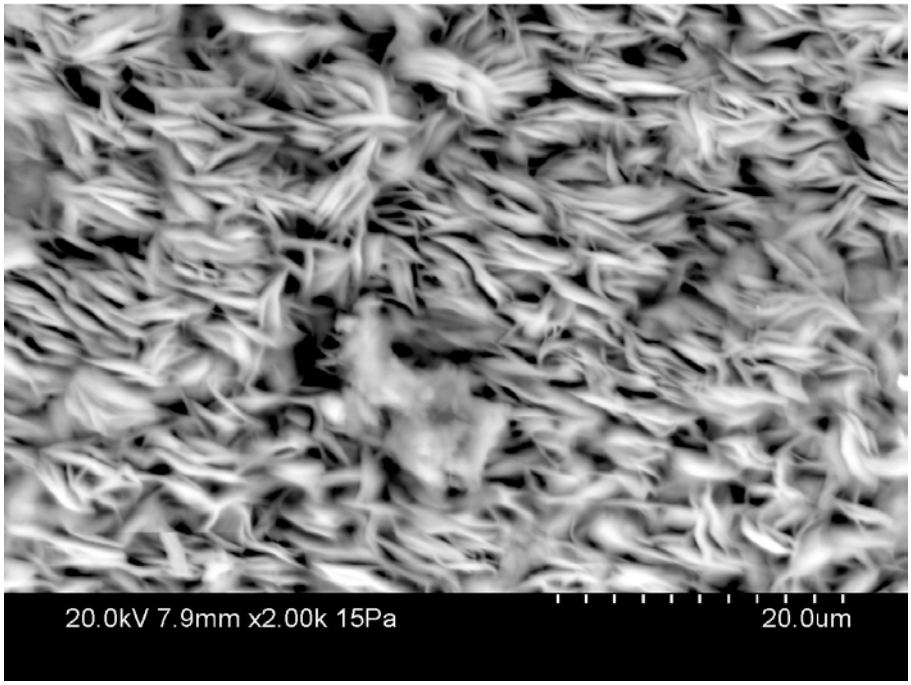

Figure A1-70. *BSE-image of mixed layer clayfrom KFR104 416.96–417.35 m.*

Borehole: KFR106

Adjusted borehole length: 9.72–9.77 m.

The fracture surface is coated with Fe-rich mixed layer clay. No iron hydroxide was found in the fracture.

Figure A1-71. *Photo of the sampled fracture from KFR106 9.72–9.77 m.*

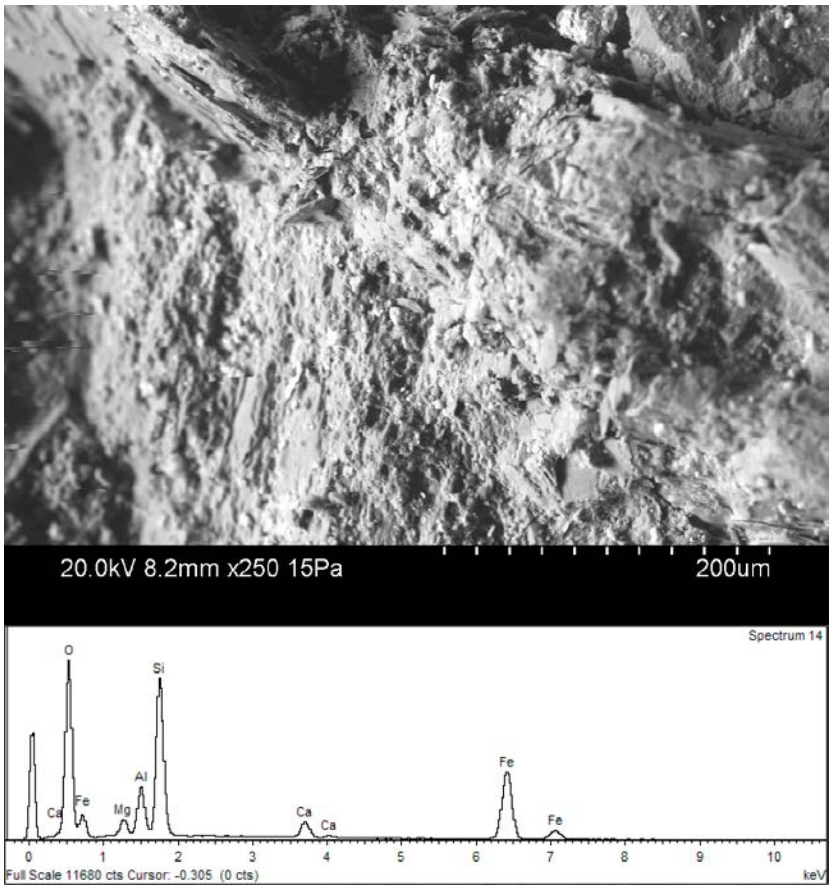

Figure A1-72. *BSE-image and EDS-spectra of mixed layer clay from KFR106 9.72–9.77 m.*